

Ignacio Fos Mira

Modelling of Thermal Management by Hybrid Channeling

Master's thesis, which has been submitted as a thesis for examination for a Final Project.

Alto University, Espoo, Finland, May 2018

Supervisor: Professor Pedro Vilaça

Advisor: Heikki Karvinen

Author Ignacio Fos Mira		
Title of Thesis Modelling of Thermal management by Hybrid Channeling		
Degree programme Mechanical Engineering		
Major/minor Mechanical Engineering	Code IA3027	
Thesis supervisor Professor Pedro Vilaça		
Thesis advisor(s) M. Sc. Tech Heikki Karvinen		
Date 28.05.2018	Number of pages 78	Language English

Abstract:

Friction Stir Welding was born as a technique to join dissimilar metals overcoming the different physical properties. The join is made in a solid state with non-consumable tools, becoming environmentally friendly. The microstructure of the new regions created during FSW shown enhanced properties too interesting for a new technique to appear, Friction Stir Processing. Based on same principles as FSW, FSP performs on metals proceeding to a microstructure refinement and so surface properties. Nevertheless, when the parameters during FSP are improperly settled, some defects emerge in the weld zone. Most outstanding one developed Friction Stir Channeling, a technique which manufactures internal closing channels by a developed tool. One step further, Hybrid Friction Stir Channeling combines, in a simultaneous action, the production of internal channels with the join of different components.

This investigation is focused on the study of the parameters involved in the proper performance and functioning of HFSC prototypes for thermal management. The adequate knowledge of these parameters leads to an optimization of HFSC application for heat removal. This dissertation considers three parameters as most relevant ones: channel roughness, thermal bridge by the weld zone and coolant velocity and temperature. Acquired knowledge about the behavior in different configurations determined by these parameters is later applied in the simulation of prototypes proposed for thermal management. Each prototype differs from others in geometry, boundary conditions, heat sources, channel path and application.

The influence of each parameter was simulated within different models. Results showed how the increase of the contact area and turbulence in the flow propitiated by roughness aid the heat transfer mechanism significantly improving heat removal. Contact surfaces are not fully contacted due to surface roughness and waviness, where the peaks leave gaps filled by air. Air low thermal conductivity act as a barrier for heat transfer. Weld zone, composed of a continuous material, avoids this resistance and aids the heat to flow through the weld zone. Easiness in heat flow means greater conduction to the coolant and lower maximum temperatures. Coolant velocity has limitations because of pump requirements and frictional losses. The higher the inlet velocity, the higher heat removal. Nonetheless, excessive velocities do not result in excellent efficiencies. There is a point from which the gain in heat removal is too deficient compared with the increase needed in the flow.

Keywords Friction Stir Welding Friction Stir Processing Friction Stir Channeling Hybrid Friction Stir Channeling Fluid Dynamic Modeling Channel Roughness Weld Zone

Acknowledgments

First, I would like to thank my supervisor, Professor Pedro Vilaça, for providing me with this opportunity to work in his project based on hybrid channeling and his continuous support, motivation and discipline required to move forward on my work. Also my advisor, Heikki Karvinen, for his effort working hand-in-hand with me every single day and his capability to make my labor go more smoothly, very implicated when I started with the new software and cheering me up. It is also remarkable the good atmosphere created by all my office mates who made easier the hard working mornings.

Finally, I cannot be thankful enough with my parents, whose support, economic and emotional, made this abroad year possible and fulfilling the objectives proposed when I came.

A handwritten signature in blue ink that reads "Ignacio Fos Mira". The signature is written in a cursive style and is underlined with a single horizontal line.

Ignacio Fos Mira

Espoo 28.05.2018

Table of contents

Abstract	
Acknowledgements	
Table of contents	6
Abbreviations	8
List of figures	9
List of tables	11
1 Introduction	12
1.1 Scope of the Thesis	12
1.2 Objectives	13
1.3 Structure of the Thesis	13
2 State of the Art	14
2.1 Historical review: friction stir welding	14
2.1.1 Process specifications	17
2.1.2 Welding	24
2.1.3 Advantages	27
2.2 Friction stir processing	27
2.2.1 FSP variables	29
2.2.2 Microstructure	31
2.3 Friction stir channeling	33
2.3.1 Channel formation	35
2.3.2 Channel shape	36
2.3.3 Channel size	38
2.3.4 Surface roughness	40
2.3.5 Hybrid friction stir channeling	41
3 Model and solver theory	46
3.1 Governing equations	47
3.2 Materials	47
3.3 Boundary conditions	48
4 Cases of study	49
4.1 Calibration with no weld case study	49
4.2 Calibration with weld case study	50
4.3 Battery plate model	50
4.4 Network system model	50
5 Fluid-dynamic modeling and analysis	50
5.1 Geometry and mesh	51
5.1.1 Models A and B	51
5.1.2 Battery Plate Model	52
5.1.3 Network Systems Model	54
6 Results and discussion	57
6.1 Basic model: influence of diverse parameters	57
6.1.1 Influence of roughness	57
6.1.2 Influence of weld zone	59
6.1.3 Influence of coolant velocity	62
6.2 Battery plate model	64
6.3 Network systems model	66
7 Conclusions	71
8 Future work	73
9 References	74

Abbreviations

TWI	The Welding Institute
HFSC	Hybrid Friction Stir Channeling
FSC	Friction Stir Channeling
FSP	Friction Stir Processing
FSW	Friction Stir Welding
NC	Non Consumable
PCBN	Polycrystalline Cubic Boron Nitride
WP	Work Piece
CTE	Coefficient of Thermal Expansion
TMAZ	Thermomechanically affected zone
WN	Weld Nugget
WP	Whorl Pin
JLR	Joint Line Remnants
IRP	Incomplete Root Penetrations
SST	Skew Stir Tool
TS	Twin Stir
CR	Counter Rotating
CDR	Continuous Dynamic Recrystallization
RSM	Rotational Shear Material
AS	Advancing Side
RS	Retreating Side
BC	Boundary Conditions

List of figures

Figure 1: Most relevant friction based processing technologies [1].	14
Figure 2: Microstructural regions in cross section of FSW material	15
Figure 3: Metallographic analysis of a FSW [4].	16
Figure 4: Microstructural regions in cross section of FSW material.	16
Figure 5: FSW basic tool.	17
Figure 6 Bottom view of shoulder geometries (Copyright© 2001, TWI Ltd).	18
Figure 7: Scrolled shoulder (left) and convex shoulder with tapered geometries (right) [14].	18
Figure 8: Round bottom pin with a concave shoulder.	19
Figure 9: Flat bottom cylindrical pin.	19
Figure 10: Truncated cone pin (left) and MX Triflute pin [20].	20
Figure 11: PCBN threadless pin tool [22].	20
Figure 12: Retractable pin-tool movement throughout weld line [24].	21
Figure 13: Comparison of surface velocities at calibration point: flat-bottom (left) and round bottom (right) [25].	21
Figure 14: FSW tool materials.	22
Figure 15: SST and detail of the pin.	23
Figure 16: Top view of weld produced by Re-Stir FSW (left) and Com-stir tool movement (right).	24
Figure 17: Different joint configurations [37].	25
Figure 18: Void imperfection in friction stir weld.	26
Figure 19: JLR imperfection in FSW.	26
Figure 20: IRP imperfection (left) and fracture caused by IRP (right).	26
Figure 21: Schematic of friction stir processing.	27
Figure 22: Patterns for FSP: (a) single linear, (b) parallel passes offset by step distance, (c) raster pattern, (d) spiral pattern [42].	28
Figure 23: Scheme of FSP.	29
Figure 24: Influence of rotational speed vs torque, aluminum alloy AlSi6Cu4.	30
Figure 25: travelling speed vs torque, aluminum alloy AlSi6Cu4.	30
Figure 26: Microstructural evolution during FSP, aluminum alloy 5083.	32
Figure 27: Al-Si section after FSP. Advancing side (AS), retreating side (RS) and rotational shear material (RSM).	32
Figure 28: Microstructure of advancing (left) and retreating (right) sides of aluminum alloy after FSP with Triflute tool.	32
Figure 29: Technological interrelations of the linear friction based manufacturing technologies [4].	33
Figure 30: Schematic of friction stir channeling.	33
Figure 31: Different process regions of a channel: channel nugget (A-B), parent material (C), channel (D), material removed from channel nugget (E).	34
Figure 32: Schematic of FSC new process [57].	35
Figure 33: Microstructural regions after FSC: base material (A), HAZ (B), TMAZ (C), stirred zone (D) and channel [58].	36
Figure 34: Different shapes at: 1100 rpm, 2.11 mm/s (a) and 1100 rpm, 2.96 mm/s (b).	37
Figure 35: Channel geometries produced with different FSC processing parameters, corresponding to Table 2.	38

Figure 36: Schematic of a channel with parameters D (closing layer thickness) and α (shear angle).	38
Figure 37: Variation of the channel area depending on traverse and rotational speeds for two different plunge depths.	39
Figure 38: Cross section of a FSC work piece showing the roughness of the channel [54].	40
Figure 39: Roughness at side walls, bottom and ceiling of FSC by four different processing parameters [62].	41
Figure 40: HFSC tool and contact region.	41
Figure 41: Cross section detail of HFSC application.	42
Figure 42: ESAB LEGIO FSW 5UT [63].	43
Figure 43: Microscopic view of two materials in contact.	44
Figure 44: Temperature drop in the joint [65].	45
Figure 45: Thermal contact resistance for aluminum 7075-T6 and copper [66].	46
Figure 46: Geometry A (above) and detail of step for geometry B (below).	51
Figure 47: Mesh detail in the inlet region. Model A (left), model B (right).	52
Figure 48: Top view of Battery Plate Model geometry and aluminum constituent bodies: type 1 (black), type 2 (yellow) and block (orange).	53
Figure 49: Mesh section and inlet detail for Battery Plate Model.	54
Figure 50: Prototype (left) and useful bodies (right) for the calculations.	55
Figure 51: Mesh detail Network Systems model.	56
Figure 52: Temperature gradient in model A and region plotted in Table 15 highlighted in black.	57
Figure 53: Temperature variation along copper and aluminum for both cases: roughness and non-roughness channel.	58
Figure 54: Turbulence kinetic energy dissipation for roughness and non-roughness channel.	59
Figure 55: Temperature gradient in model B and detail of temperatures plotted (black lines).	60
Figure 56: Maximum temperatures across body length for model B.	61
Figure 57: Temperature drop at inlet and outlet for weld and interface models.	62
Figure 58: Heat transfer throughout the weld zone.	62
Figure 59: Temperature variation in copper for different inlet velocities.	63
Figure 60: Detail of inlet/outlet path and weld zone aluminum-copper in bottom.	64
Figure 61: Temperatures in copper plate.	64
Figure 62: Aluminum parts temperature gradient in Battery Plate Model.	65
Figure 63: Plots of temperature variation throughout colored lines: above chart (black line), below chart (purple lines).	65
Figure 64: Flow temperature (left) and velocity streamlines showing reverse flow (right) at inlet and outlet.	66
Figure 65: Power electronics location.	67
Figure 66: Temperatures in copper components for 1 m/s (left) and 0.5 m/s (right).	67
Figure 67: Temperature gradient through power electronic and contact with copper plate.	68
Figure 68: Pressure variation along coolant domain.	68
Figure 69: Velocity variation within channel curves: slow velocities (green regions) and fast velocities (orange regions).	69
Figure 70: Velocity variation in curve and straight sections (cross section view).	69
Figure 71: Network Systems prototype maximum temperatures cooled by OptiCool.	70
Figure 72: Coolant temperature variation: OptiCool (left) and water (right).	70

List of tables

Table 1: Advantages of FSW [16].	27
Table 2: FSC process parameters [61].	37
Table 3: FSC channel areas for different conditions [61].	40
Table 4: Factors influencing thermal contact resistance.	43
Table 5: Liquid cooling properties [69].	48
Table 6: Solid material properties [69].	48
Table 7: Dimensions for model A.	51
Table 8: Dimensions for model B.	51
Table 9: Mesh statics for model A.	52
Table 10 Mesh statics for model B.	52
Table 11: Dimensions for Battery Plate Model.	53
Table 12 Mesh statics for Battery Plate Model.	54
Table 13: Geometrical data for Network Systems model.	55
Table 14: Mesh statics for Network Systems model.	56
Table 15: Difference in maximum temperature for each material.	58
Table 16: Power values for each component.	67
Table 17: Maximum temperatures in each body for different conditions.	70

1 Introduction

As we know, in most processes that take place today going from driving a car, using the mobile phone or especially in industrial processes, energy is generated in the form of heat. Occasionally, this heat can adversely affect the performance of the process or produce undesirable conditions. Heat exchangers play a fundamental role in heat dissipation since they are the necessary element to maintain the temperature in a permissible range. The variety of systems that need heat removal obliged to foster the creation of a broad range of heat exchangers. The versatility of a heat exchanger resides in several factors such as geometry, materials, size and dissipated power. Manufacturing techniques look forward meeting all these factors for a polyvalent use of heat exchangers.

Hybrid friction stir channel broke down heat exchangers industry with an innovative technique consisting in a simultaneous action to weld different materials and form internal channels. The technique is able to produce infinity alternative paths by a non-consumable tool in an efficient and environmentally friendly process. Simplicity and versatility of the process raised HFSC to be highly competitive with alternative techniques.

The usage of materials such as copper and aluminum create an ideal field for the heat movement at the same time as weight and costs are saved. Channels manufactured allow any fluid to flow inside the machined metal to be cooled down.

HFSC opened new possibilities in the design and manufacturing of new prototypes for several applications on a large and small scale. Knowledge of parameters involved in its performance and improvements in production are key on the establishment at industry.

1.1 *Scope of the Thesis*

This thesis details the evolution from FSW to HFSC and the incorporation of this last one technique to the manufacturing of thermal management prototypes. HFSC combines the techniques from FSW and FSC for producing continuous internal closed channels and welding of different metal plates. Tools utilized in both FSW and FSC processes are developed to make unique designs favoring distinct material flows to encourage channel formation.

The usage of materials such as copper and aluminum, with high thermal conductivity, make HFSC prototypes feasible for thermal management. Combination of both metals has remarkable advantages. Fully copper prototypes suppose excessive weight and costs, but its thermal conductivity makes it ideal for heat distribution in contact con devices to be cooled down. Aluminum prototypes are lighter and cheaper but, in terms of thermal conductivity, efficiency is lower than copper. Channels let any fluid to flow unhindered through the inside, widen versatility for any application. Inner roughness increase surface area and promotes turbulent flows in the coolant media which is useful for the heat transfer in the interface. These properties and the economic field place HFSC in the top in relation to alternative heat exchangers manufacturing techniques.

To better understand and optimize the process parameters in HFSC prototypes. Prototypes geometry and design are restricted to customer requirements. Thus, effectiveness will depend on boundary conditions and the proper configuration of parameters. Simulations are

critical to demonstrate the suitability of HFSC for thermal management and the influence of its characteristics.

1.2 **Objectives**

The main objective of the thesis is to study and understand the benefits of using hybrid friction stir channeling for heat transfer applications. Once the involved parameters are identified, the work will focus on their relevance in the heat exchanger performance including the optimal values for an efficient heat removal. If there is time, the validation of the model will be done at the laboratory. Main steps to proceed in the thesis are.

- Previous knowledge: understand and learn the physics and development of the FSW, FSP and FSC as previous techniques with the same procedure basis as HSFC.
- Acknowledge HFSC advantages and disadvantages as well as its performance.
- Design using CREO/CAD of the model and geometry to be used as a model to analyze the parameters intervening in the proper functioning of HFSC heat exchangers.
- Determination of the materials to be used. Since the project is already in progress, chosen materials are copper, aluminum and a fluid (water or air).
- Evaluate the model performance under the defined boundary conditions using a Finite Element Method simulation of the component.
- Analyze the solution and look for possible changes to improve performance within the current techniques.
- To build a prototype with the specified dimensions and materials.
- Evaluate the component behavior in a real test and compare with expected results.

1.3 **Structure of the Thesis**

Next to the present introduction, State of the Art is the second chapter. It includes an extensive and comprehensive literature review on the techniques which later developed into hybrid friction stir channeling. There are detailed the procedures and variables taken from each technique to better understand HFSC: process specifications from FSW, microstructure resulting from FSP and channel characteristics in FSC. Finally, HFSC is briefly described as the method used in our prototypes manufacturing.

Chapter three explains the fluid-dynamic modeling used in the later simulations, including all the information concerning the software theory and its application to the prototypes, such as governing equations, geometry or meshing properties.

Chapter four describes the case of study, explaining in a few words the models chosen to analyze HFSC effectiveness and feasibility for heat extraction. Also, de prototypes studied are explained.

Chapter five contains the details about geometry and mesh for every model.

Chapter six includes the results and analysis from the study of the different parameters involved in heat extraction effectivity for HFSC, looking for its optimization and demonstrating advantages faced to alternative technologies. Also, results of the performance for different prototypes are described and examined.

Finally, chapters seven and eight summarize the work and add recommendations for possible future work.

2 State of the Art

This chapter presents a literature review where the basis of FSW, FSP and FSC processes are explained. This is needed to purchase the required knowledge to understand how the processes work and allow a precise calculation to obtain the expected results.

2.1 Historical review: friction stir welding

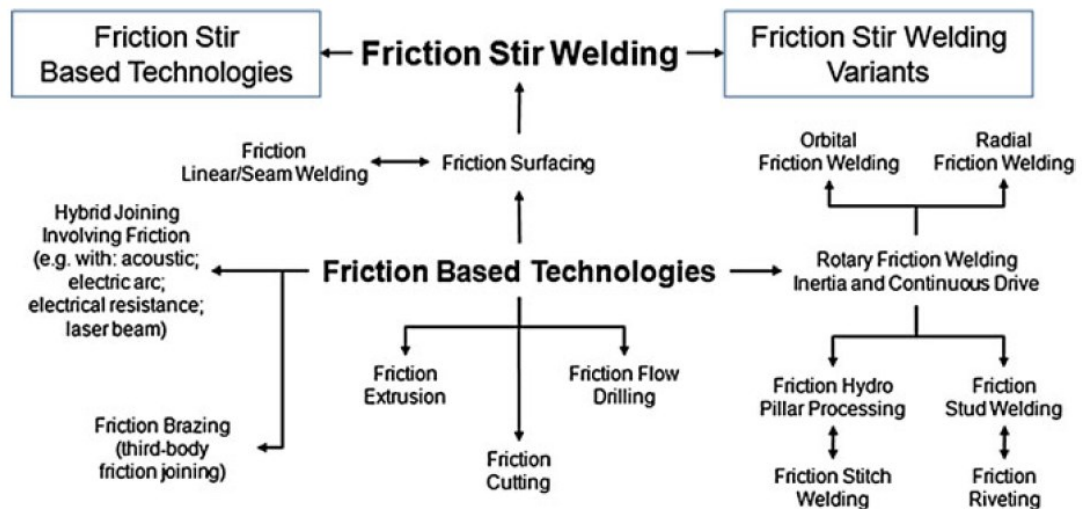


Figure 1: Most relevant friction based processing technologies [1].

FSW is a procedure patented in 1991 by Wayne Thomas at The Welding Institute, which allows joining solids, mainly metallic alloys, that can be difficultly joined by using other methods [2]. Not melting the solids is the principal difference in relation to other welding processes, an important advantage when welding different alloys since can be coupled without care about any issue related with fusion welding (solidification or composition harmony) [3]. FSW consumes less energy, no consumables used (such as flux or cover gas) and no noxious emissions are released. Consequently, the process is energy sustainable, environment-friendly, adaptable and creates enhanced joint properties. This technique is based on a non-consumable rotation tool inserted into a butt joint between two solids and moved forward along the join at a determined speed. Thanks to the non-consumable tool, no material is added so there is a save in filler material and thus less final weight.

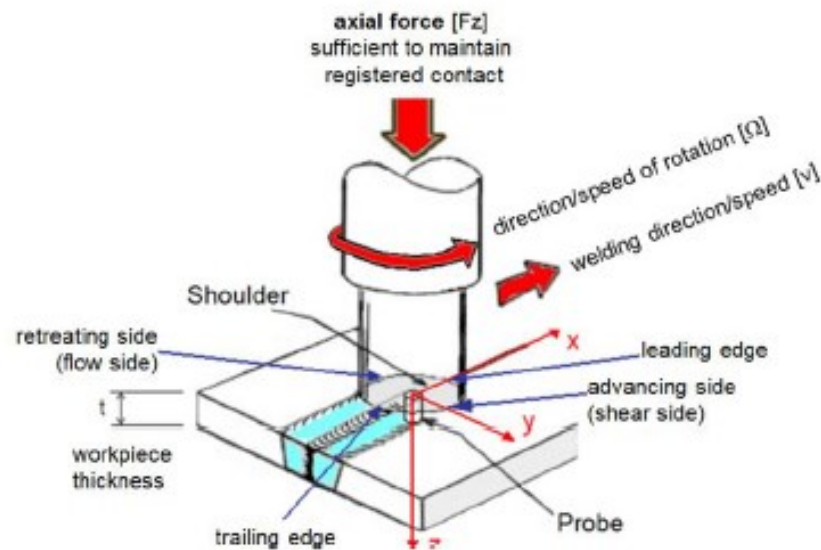


Figure 1: Friction Stir Welding parts [4].

As seen in Figure 1, the NC tool consists in a massive cylinder with an expressly designed shoulder and a pin at the bottom pushed against the metal surfaces. A downward force is applied to the tool combined with a rotation movement until the pin penetrates into the material in the joining and the contact between surfaces is produced.

Keeping both rotation and vertical force, the tool is transported along the piece. Throughout this movement heat is produced, the temperature in the weld zone increases due to friction and results in a strong plastic deformation. Usually, reached temperature is not enough to melt the solids, forming a joint in a solid state. Moreover, the softened area around the pin suffers deformation resistance decrease, product of high temperature plastic deformation, leading to a remarkable microstructural evolution to fine, equiaxed and fully recrystallized grains. As consequence, this microstructure contributes with great mechanical and fatigue properties, improved formability and extraordinary super plasticity [5]. Thanks to the softening, the rotation movement moves material from the front to the back of the pin. Nevertheless, this creates a cavity which instantly is effectively filled with the material pushed by the shoulder, which provides confinement for the material. That is why shoulder is designed to create deformational and frictional heat in thin leaves while the pin is in charge of thick pieces [6] [7].

Material movement in the joint region can be very complex resulting in a not homogeneous zone as consequence of gradient strains and temperature [8]. Post welding microstructure regions require a new nomenclature to identify them:

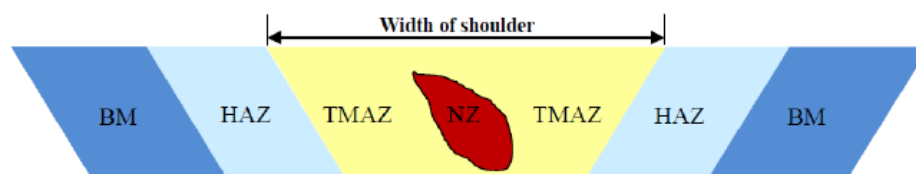


Figure 2: Microstructural regions in cross section of FSW material¹

¹ Source: https://www.researchgate.net/figure/Welding-zones-after-FSW-process_fig6_274007963

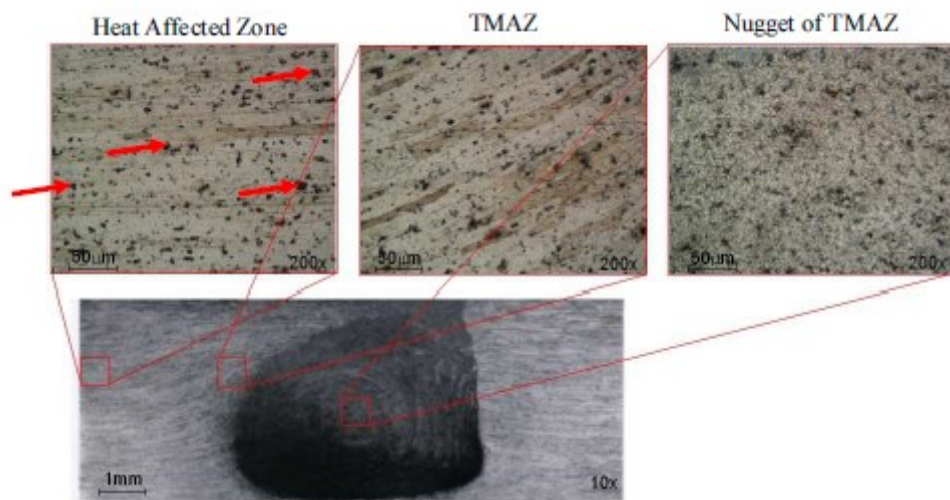


Figure 3: Metallographic analysis of a FSW [4].

- **Unaffected material:** this region corresponds to the material far away from the weld zone, where it is not affected by the heat in reference to mechanical or microstructural properties, preserving all its original characteristics.
- **Heat affected zone:** HAZ, located next to the unaffected material, and closer to the weld. Heat induces a thermal cycle to the material modifying mechanical properties or microstructure, but no plastic deformation happens in this region.
- **Thermomechanically affected zone:** TMAZ, next to HAZ. The material is characterized by its plastic deformation exerted by the tool movement. Moreover, thanks to the influence of heat is viable to get plastic strain without recrystallization, highlighting the boundary between TMAZ and next area.
- **Weld nugget:** also called stir zone, in the epicenter of the welding through the tool pin has swept. Unlike TMAZ, WN is completely crystallized.

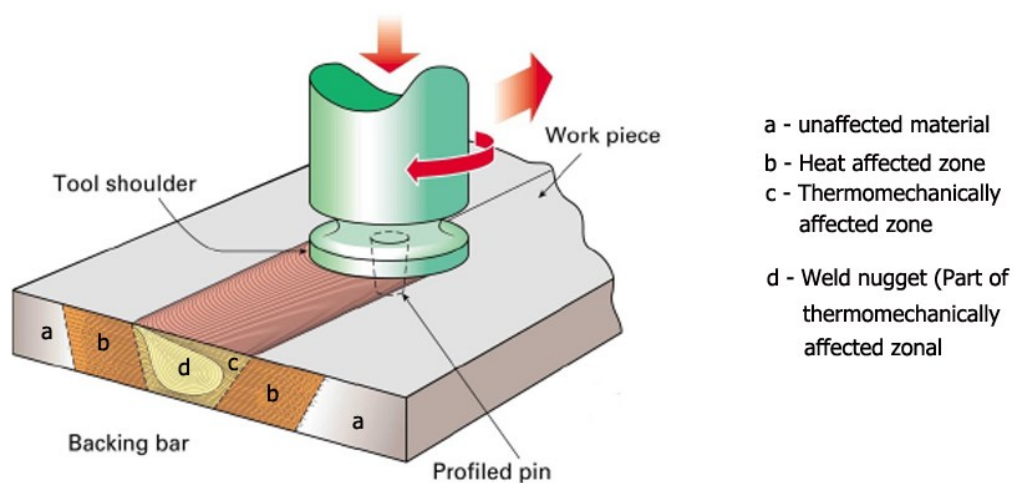


Figure 4: Microstructural regions in cross section of FSW material².

² Source: https://www.researchgate.net/figure/Welding-zones-after-FSW-process_fig6_274007963

2.1.1 Process specifications

2.1.1.1 Tool design

Tool consists of a pin and a shoulder. Pin contact with the work piece produces friction and deformation releasing heat to soften the WP, while the shoulder contact expands the softened material, increases the produced heat and hold down the deformed material. Their specifications are probably the most determining aspect in the proper development and functioning. Tools are configured aiming three goals:

1. Soften the materials by generating local heat (primary from friction and once the movement starts, also by deformation).
2. Control material movement and flow.
3. Hold the hot material under the shoulder.

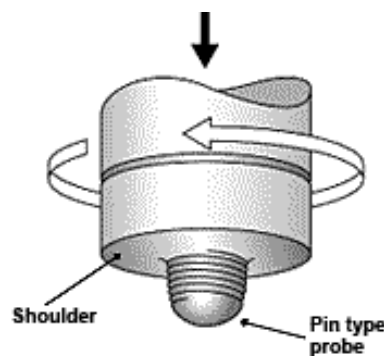


Figure 5: FSW basic tool³.

As FSW use is extended, experience and understanding of the process lead to evolved notably tool geometry. Some deeply studied features added to the tool look for an improvement altering flow of material or stresses.

2.1.1.1.1 Shoulders

First shoulder design was concave (standard type) and still the most popular design thanks to its simplicity and ease of machining [9]. Appropriate use of this design needs tilting the tool 2 to 4° from the WP normal even if there are corners. Also, different shoulder profiles were developed in TWI to fit in any circumstance. Inserting re-entrant features, as seen in Figure 6, the tool confines more plasticized material and improves coupling with WP, resulting in high quality stir welds [10]. Developed features can be mechanized in any shoulder profile (convex, flat or convex) and basically consist of spirals, grooves, circles or crests [11] [12].

³ Source: https://www.researchgate.net/figure/Model-of-the-first-tool-used-in-friction-stir-welding-2-100_fig2_320434388

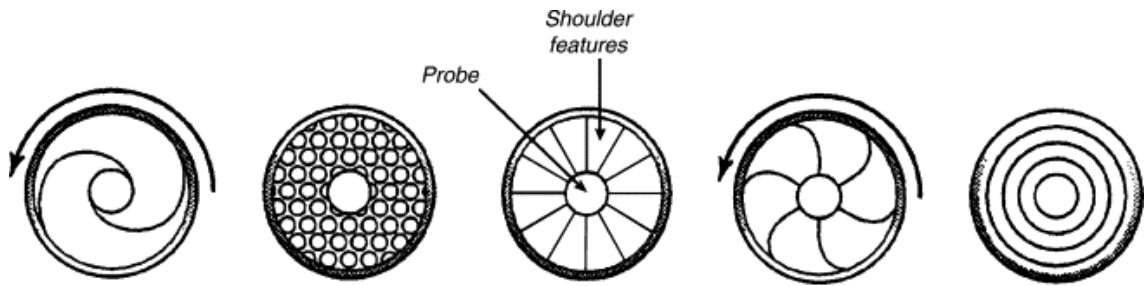


Figure 6 Bottom view of shoulder geometries (Copyright© 2001, TWI Ltd)⁴.

Among these features, most extended one is spiral shoulders, known as scroll shoulder. Its configuration is based on a flat surface where a channel is machined from the edge to the center, acquiring spiral shape. This feature eliminates the needs of tilting the spindle thus more complicated patterns can be welded and the stirring device design gets simplified. Furthermore, compared with concave tools, contributes with significant flash reduction, higher welding speeds and reduces the load required to get a good contact with the WP [12].

On the other hand, the use of convex shoulders has always been very limited due to the inability to hold the stirred material under the shoulder. Despite this limitation, main advantage resides in the capability to be engaged to the WP at any place since the outer edge of the shoulder does not need to interlock with WP. This increases the flexibility on contact area (vary the amount of engagement with WP does not carry losing weld quality), provides ease to join different thickness WP, improves imbalance tolerance and enhance ability in welding difficult curvatures [13].

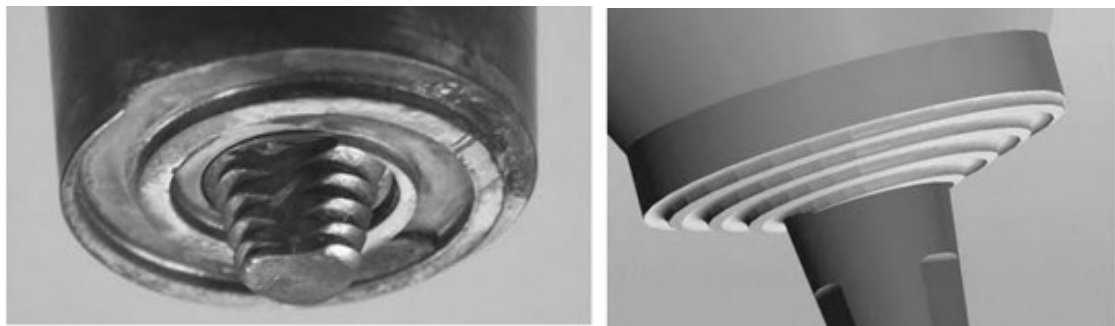


Figure 7: Scrolled shoulder (left) and convex shoulder with tapered geometries (right) [14].

2.1.1.1.2 Pin

Pin is in charge of producing heat in the joint surfaces by deforming and friction materials. Its design determines depth, process speed and should accomplish break WP surface to later stir and move the softened material to the back of the tool. As happens with shoulders, experience and investigation lead to revolutionary designs and improved performance. Some designs are briefly explained down below:

⁴Source: <https://www.scopus.com/record/display.uri?eid=2-s2.0-0043062679&origin=inward&txGid=55bcdbe12b6b641d7f34fcc15e6154ea>

- **Round-Bottom Cylindrical Pin:** used in the first FSW patent [9], characterized by a threaded surface and a round bottom. This surface feature transports the material from the upper to the bottom part of the pin. The domed pin end attenuates tool wear and ameliorates weld root quality. As demonstrated in [15], optimum dome radius was set as 75% of pin diameter. As this radius is decreased, the bigger feasibility to produce low quality welds.



Figure 8: Round bottom pin with a concave shoulder.

- **Flat-bottom Cylindrical Pin:** most popular design. The reason to use a flat bottom instead of a domed one resides in a geometrical issue. The highest local surface velocity takes place on the cylinder's edge, so these values are higher as the pin radius is reduced (Figure 9). As consequence, higher surface velocity provides the pin greater disposal to affect the material located under the pin, even if they are not in touch.

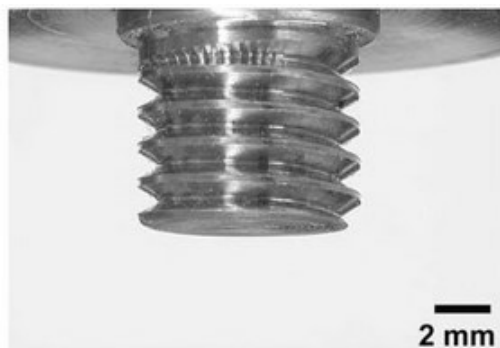


Figure 9: Flat bottom cylindrical pin.

- **Truncated Cone Pin:** this design arose from the need to apply FSW in thicker sheets and in faster travel velocities. It is an uncomplicated evolution of cylindrical pin, contributing with lower transverse loads and displacing moment loads to the strongest region, the base of the cone [16] [17] [18].
- **Addition of Machined Flats on Pins:** the addition of flat surfaces modifies material transfer around the pin by producing a turbulent plasticized material flow which locally increases the material deformation [11]. The experiment took by [19] comparing three different tools demonstrated how effective were the flats increasing the weld nugget area and WP temperature.
- **Whorl Pin:** evolution developed by TWI. When performing, WP reduces 60% of the displaced volume besides transverse loads and enabling higher tool travel speeds compared to a cylindrical pin with same diameter. Moreover, has a good ratio

volume swept/pin volume: 1.1 for cylindrical pins while 1.8 for WP. The main difference with truncated cone resides in helical ridge pattern which performs as an auger creating a downward move [20].

- **MX Triflute Pin:** upgrading WP, MX Triflute was achieved. Adding three different flutes cut into the ridge displaced volume is even higher (70%) and provides supplementary deformation during the weld [21]. Volume ratio is up to 2.6 and increases travel speed 2.5 times over preceding model.

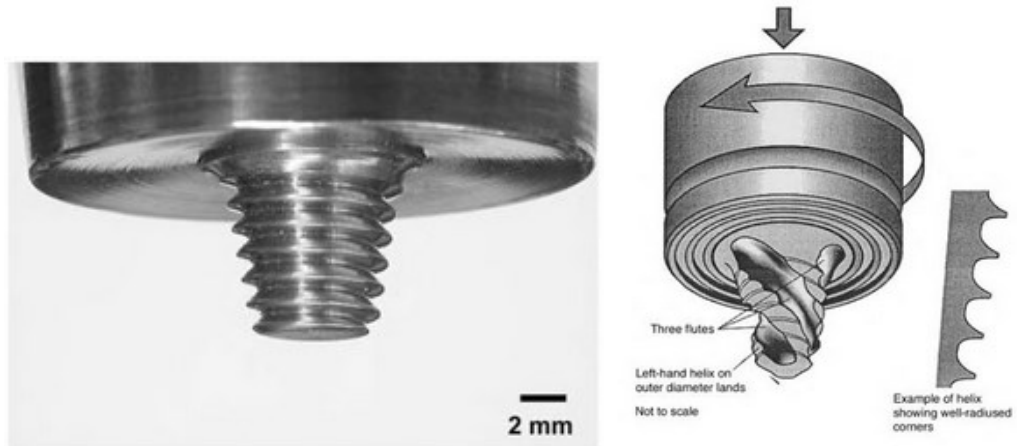


Figure 10: Truncated cone pin (left) and MX Triflute pin [20].

- **Threadless pin:** operating in extreme conditions such as high temperatures or hugely abrasive alloys might not be suitable for threaded features because of and disproportionate wear or fracture and so a short lifetime. Instead, these designs for aggressive conditions are simple models with strong features.



Figure 11: PCBN threadless pin tool [22].

- **Retractable Pins:** as its name suggest, these tools are characterized by an adaptable pin to modify length plunge to the WP during FSW. Is a suitable solution in the face of welding WP with thickness variation and allows the closure of the exit hole in some FSW retracting the pin as the tool reaches the end of the weld [23].

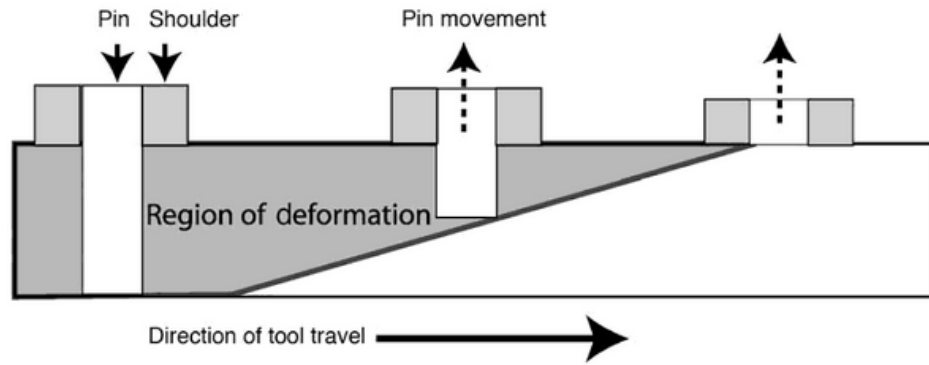


Figure 12: Retractable pin-tool movement throughout weld line [24].

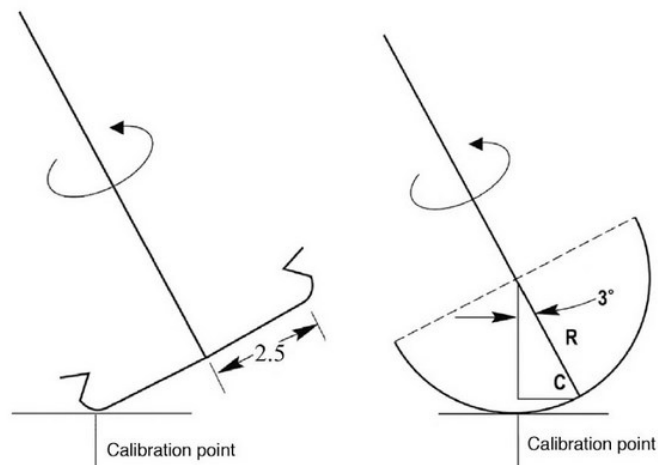


Figure 13: Comparison of surface velocities at calibration point: flat-bottom (left) and round bottom (right) [25].

2.1.1.1.3 Materials

Due to working conditions, tool material must be robust, durable and hard to wear at high temperatures. Low thermal conductivity and oxidation resistance are also desirable to mitigate damage and heat loss to the tool. Apart from work piece material, there are some others considerations to take care when defining tool material [26]:

- **High temperature strength:** the aspirant material should be able to resist the loads generated when it makes the first contact with the piece and cut resistance to avoid fracture during stir welding. Since prophesy the required strength requires entangled computational simulations, usually the selection is based on experience.
- **High temperature stability:** good creep resistance is important, especially in lengthy welds, where tool dimension changes can take place. Annealing, overaging and dislocation substructures provoke changes in mechanical properties enabling shape modification or fracture.
- **Wear resistance:** clearly, excessive wear finish in shape alteration, therefore, the weld quality decreases and facilitates the appearance of defects. During friction stirring, wear can be done by three mechanisms: abrasive, chemical or adhesive wear. Which one will appear depends on factors such as tool parameters and the interplay between the tool and work piece, e.g., in PCBN tools low rotation speed

enforces adhesive wear while in high rotation speeds causes wear is because of abrasive wear [27].

- **Tool reactivity:** any reactivity from the tool, either with the environment or the work piece, is undesirable, negatively affecting both surface tool properties and join quality. Toxic substances like MgO_3 can be released, needing cover gases to mitigate the effect, also used to protect work piece from oxidation.
- **Fracture toughness:** tool plunge is a determining factor when talking about fracture. Despite applying different methods to mitigate those effects (pilot hole, pre-heating WP or slow plunge velocity) [28], first touch with the WP produces local stresses that can easily break the pin, in addition to the spindle lateral movement during rotation which also must be considered.
- **CTE:** considering multi-material tools (distinct material for shoulder and pin), great differences in the CTE might lead to the expansion of the shoulder relative to the pin and vice versa. Any of these cases raise stresses in the interface favoring tool breakdown. Even more attention is needed when shoulder and pin are the same material while tool shank is different. This situation can be mitigated using a thermal barrier to avoid heat moving from the tool to the shank, as it is applied in PCBN tools [29].
- **Machinability:** many tools have features that must be compatible with the selected material.
- **Material availability:** It is unprofitable not to have a continuous supply of tool material.
- **Uniformity in Microstructure and Density:** a small region where density or microstructure is not continuous weakens the material and is a focus for early fracture. Thus, tools are made from a fully dense grade.

Alloy	Thickness		Tool material
	mm	in.	
Aluminum alloys	<12	<0.5	Tool steel, WC-Co MP159
	<26	<1.02	
Magnesium alloys	<6	<0.24	Tool steel, WC
Copper and copper alloys	<50	<2.0	Nickel alloys, PCBN(a), tungsten alloys
	<11	<0.4	
Titanium alloys	<6	<0.24	Tool steel
Stainless steels	<6	<0.24	Tungsten alloys
Low-alloy steel	<6	<0.24	PCBN, tungsten alloys
Nickel alloys	<10	<0.4	WC, PCBN
	<6	<0.24	PCBN

(a) PCBN, polycrystalline cubic boron nitride

Figure 14: FSW tool materials.

2.1.1.1.4 Complex tools

In order to achieve more effective and efficient processes, TWI pushed new complex motion tools design which increases travel speed, material volume swept or the weld

symmetry. These developments are more focused in tool motion than in pin design. Following this line, skew stir tools obtain excellent volume swept by offsetting the pin's axis from the axis of the spindle. This offset generates an orbital motion that widens the action area and originates more deformation [30] [31]. The orbital movement reduces up to a little portion the contact between the pin and WP taking the advantage of removing the inside part of the tool, as seen in Figure 15. WN produced is wider than the pin diameter and incidence of root defects is lower.

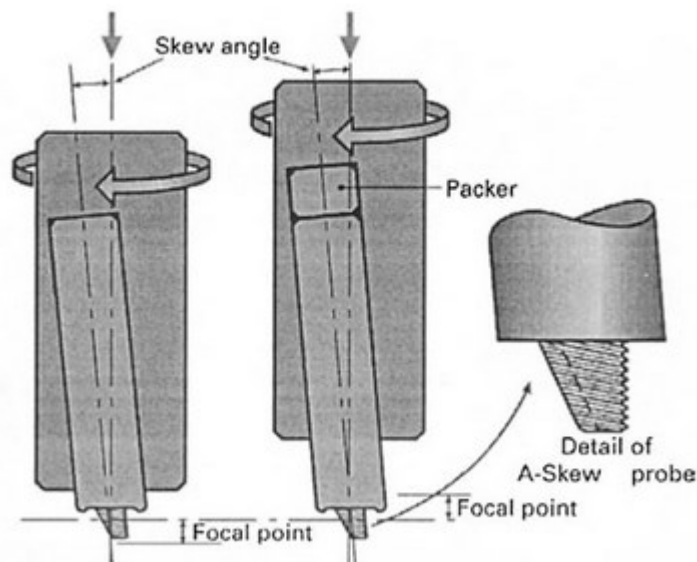


Figure 15: SST and detail of the pin.

Com-stir tools (Figure 16) are the result of combining this orbital motion with shoulder rotatory motion. Amount of swept material is even higher as well as the weld width and oxide fragmentation on the surfaces are. Torque is reduced so the necessary fixturing is simpler [32]. Re-stir tools eliminates the intrinsic asymmetry of FSW by alternating rotation movement. Thus, retreating and advancing areas change their position during the welding and a characteristic symmetric weld is formed (Figure 16) [33]. Instead, in dual-rotation tools pin and shoulder act as independent bodies. The both rotate at different speeds or directions. Because of differences in the diameter, velocity at the edge of the shoulder is higher than at the edge of the pin. In some cases, for a determined pin's velocity the corresponding shoulder velocity might be too high and cause overheating in the WP. This issue allows to synchronize the velocity at the edge of the pin and the shoulder (or even rotate the pin faster than the shoulder) avoiding overheating and its resulting defects [34]. If we go further, efficiency and speed can raise more when using more than one FSW tools. In thick plates, two counterrotating tools reduce the torque in the WP and thus fixturing needed to fasten the piece [35]. Currently, this concept is evolved in TWI known as Twin-Stir, where three variations are considered. Parallel TS is used for lap welds by two side by side CR tools. This technique displace the thinning defects to the region between two tools, so mechanical properties are not affected. Tandem TR uses two faced tools (with CR or not) to achieve, as usually, fixturing reduction, higher welding speed and deformation of the faying surfaces. Lastly, third variation consists in two staggered tools, but slightly displaced to the side, obtaining benefits thanks to the increased oxide dispersion and a very wide WN.

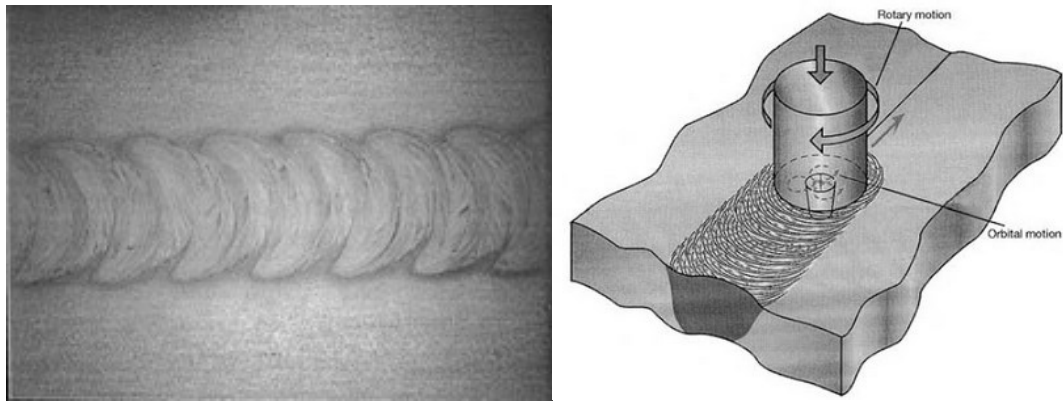


Figure 16: Top view of weld produced by Re-Stir FSW (left) and Com-stir tool movement (right).

2.1.2 Welding

The quality of the weld in FSW is closely related with two parameters: tool traverse (v) alongside the union and rotation (ω) speeds. Rotation can be clockwise or counterclockwise depending on the welding path. As said before, the rotation is in charge of mixing and blending WP material in the pin surroundings while translation movement displaces the blended material from front to rear of the tool, completing welding process. The higher rotation speed is, the higher the friction heating, outcoming deep mixing and stirring. Nevertheless, this speed increase will not always affect temperature with the same intensity since there is a variation in the coefficient of friction between tool and WP.

Besides mentioned parameters, we can also manage two additional aspects. It is not necessary that the tool is in perpendicular position to the work area. With an appropriate angle between the spindle and the WP surface is guaranteed material holding under the shoulder and its movement to the back of the pin. Concerning the pin, depth penetration into the WP is decisive when using smooth shoulders to produce good welds. When pin insertion is too slight it won't be contact from the shoulder to the WP, causing stirred material movement failure, generating welds with grooved surfaces or internal channels (these inner channels, however, can be very profitable for other applications as we will see later). If, instead, pin insertion is excessively deep, shoulder contact is too strong creating a concave weld and creates too much flash.

Lastly, some FSW processes might need preheating or cooling. This is necessary when using welding materials with high melting (steel) point or conductivity (copper), because stirring movement could not be enough to soften the WP around the pin and produce flawless welds. Supplementary heat can aid the process likewise using additional cooling when working with low melting point materials.

2.1.2.1 Joint configurations and imperfections

FSW can be applied through a myriad of geometrical shapes and diverse types of joints like T-butt, lap or butt joints [36], being last two ones the most favorable ones. Typical procedure for FSW starts with placing the sheets to be welded on a backing plate, firmly

tied to ensure any relative displacement especially during the initial plunge where the applied forces are the greater. Process preparation is very simple for butt and lap joints and combining these two configurations many others can be done, as summed up in next table. The disposition of the faying surfaces must fit with tool features thus this orientations helps the tool traverse movement. There is no even need to concern about surface quality.


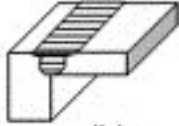
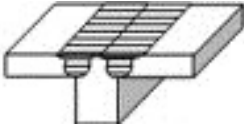


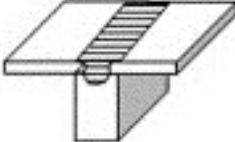
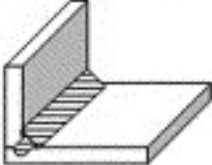
Joint configuration	
Square butt	
Edge butt	
T butt joint	
Lap joint	
Multiple lap joint	
T lap joint	
Fillet joint	

Figure 17: Different joint configurations [37].

FSW suffer from three typical imperfections: voids, joint line remnants and incomplete root penetrations. Voids are easy to detect by non-destructive testing methods. Nevertheless, JLR and IRP might be hard to find [38]. FSW tool design parameters (speeds, design, tool tilt, pin penetration etc.) not only are selected on the bases of the application required. They also affect the quality of the weld and this highly influences in the final design.

1. **Void:** usually found in the advancing face of the weld, under to the surface or through it (Figure 18). It is caused by lack of forging pressure, great welding speed and not enough WP clamping [39]. The softened material is supposed to be able to fill the void formed by the pin. If any of pin design or travel speed are incorrectly configured the material gets cooled before fill the whole gap behind the tool. Same happens with the shoulder: poor heat generated, incorrect pressure or diameter worse material flow and generates voids.

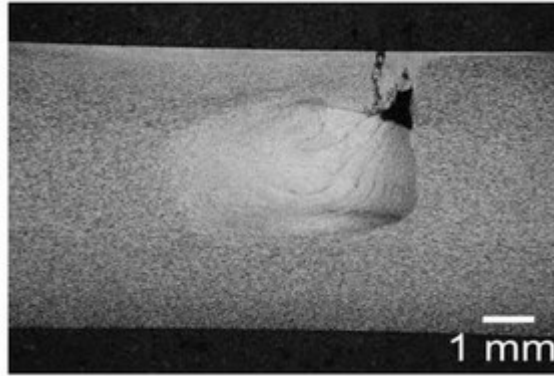


Figure 18: Void imperfection in friction stir weld.

2. **JLR:** also known as lazy S, takes place when a semi continuous layer of oxide appears through the weld nugget (Figure 19). This oxide layer was originally in the faying surfaces of the pieces to be joined. They are caused because of insufficient cleaning before welding or poor deformation at the surface, high welding speed and excessive shoulder diameter [39].
3. **IRP:** triggered by variations in WP thickness, insufficient alignment between tool and joint interface or incorrect tool design. If the pin is too far from the supporting anvil, the region grasped within the bottom of the tool and plate surface is undeformed. FSW requires a proper depth of deformation to avoid IRP (Figure 20).



Figure 19: JLR imperfection in FSW.

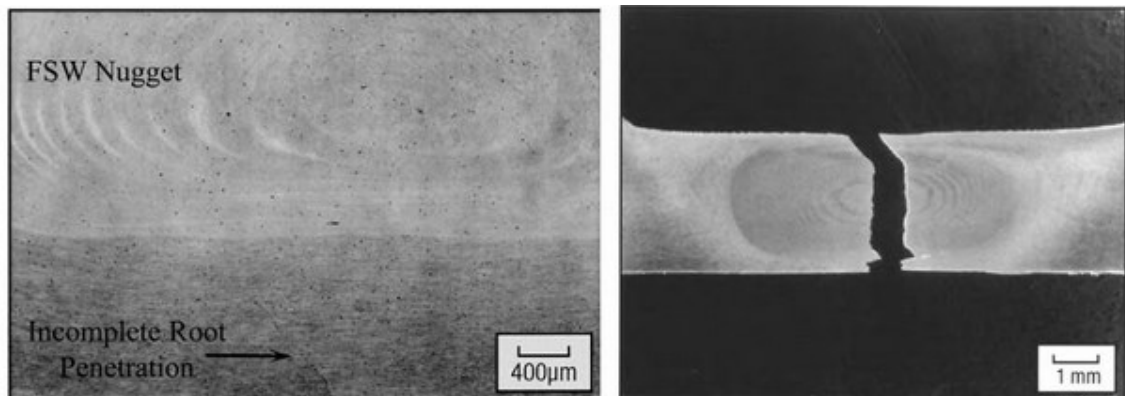


Figure 20: IRP imperfection (left) and fracture caused by IRP (right).

2.1.3 Advantages

The next table summarizes the main advantages of applying FSW across several areas:

Metallurgical benefits	Environmental benefits	Energy benefits
Solid state process	No shielding gas required	Improved materials use allows reduction in weight
Low distortion of workpiece	Minimal surface cleaning required	only 2.5% of the energy needed for a laser weld
Good dimensional stability and repeatability	Eliminate grinding wastes	Decreased fuel consumption in light weight aircraft, automotive and ship applications
No loss of alloying elements	Eliminate solvents required for degreasing	
Excellent metallurgical properties in the joint area	Consumable materials saving, such as rags, wire or any other gases	
Fine recrystallized microstructure	No harmful emissions	
Absence of solidification cracking		
Replace multiple parts joined by fasteners		
Weld aluminium alloys		
Post-FSW formability		

Table 1: Advantages of FSW [16].

2.2 Friction stir processing

Friction stir processing takes as its underlying principle the ones coming from FSW. Nevertheless, FSP does not consist in joining pieces by the weld nugget. It is a surface technology which purpose is to modify the local microstructure eliminating defects and getting new enhanced properties. It was developed by Mishra in 2000 and there are great expectations concerning microstructure refinement [40].

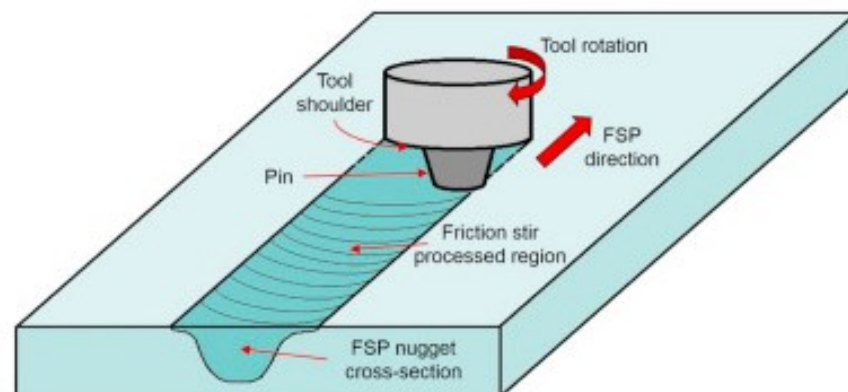


Figure 21: Schematic of friction stir processing⁵.

In the same way as in FSW, the pin is plunged into the desired material until the contact with the shoulder bottom part. Once inside, the tool, combined with rotation movement,

⁵ Source: <https://www.sciencedirect.com/science/article/pii/S0921509318300534>

moves throughout the WP. Loads exerted heat the material and result in a material flow, plastic deformation and high temperature. Most process characteristics are the same in FSW and FSP, but differences lie in the interest areas: for FSP are the regions within stir zone and TMAZ, which determines the properties of the modified area, and the region immediately under the pin. Main design parameters for FSP:

1. Rotational and travel velocities.
2. Tilt angle
3. Pin penetration depth
4. Tool geometry and dimension
5. WP material
6. Cooling and clamping system.

Despite the width of the weld zone is a little bigger than the pin diameter, sometimes is not enough to cover the needs. Therefore, there are two possibilities to widen the affected zone. First, by simply increasing tool diameter, which entails more torque and so more power demand. Second, by using multi run FSP slightly overlapping the successive passes to guarantee demanded properties [41], expanding the surface subjected to the thermo-mechanical cycle. When looking at the working area, microstructure gradients can be observed, usually more notable in the advancing side than the retreating side. This is due to the asymmetrical deformation produced by the tool rotation. To this issue, parallel traverses as seen in Figure 22.b achieve replacements of the advancing with retreating interfaces. By the other hand, pattern followed in Figure 22.c clusters the advancing and retreating interfaces in a transverse direction to the tool advance. Finally, Figure 22.d also replaces advancing interfaces with retreating ones in a spiral pattern which might mitigate gradients in the stir zone. Step distances in the successive passes are function of tool diameter. Excessive steps result in unfinished overlapping driving to microstructure gradients. Make passes with step distance of approximately 0.5 of the pin diameter avoids microstructure gradients [42].

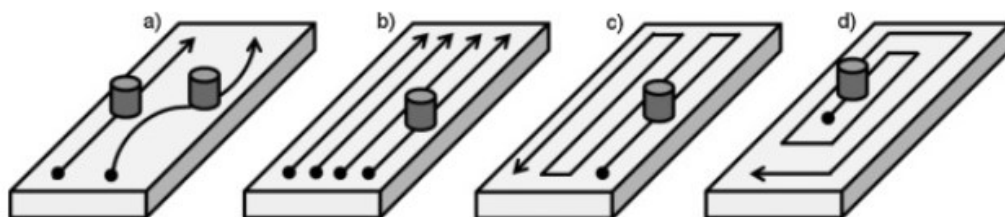


Figure 22: Patterns for FSP: (a) single linear, (b) parallel passes offset by step distance, (c) raster pattern, (d) spiral pattern [42].

Thanks to its simplicity, FSP is very effective for several applications [43]:

- Enhance corrosion resistance and mechanical properties.
- Resultant microstructure with refined grain
- Superplastic materials and special alloys production.
- Reduction of porosity.
- Variety of applicable materials: aluminum and magnesium alloys, copper, titanium and others.

As in FSW, issues such as tool dimension, pin shape, penetration and diameter, WP material or speeds have an important role. Most significant loads in FSP are axial (F_z), traverse (F_x), side (F_y) forces and torque (M_z) (Figure 23). All these parameters must be properly selected to succeed in achieving defect-free areas [44].

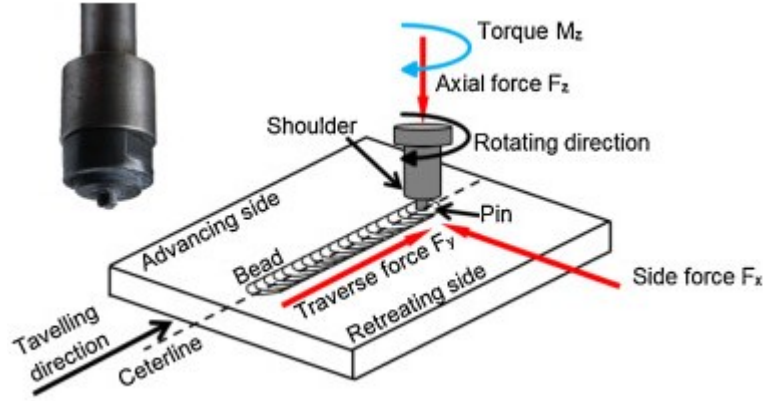


Figure 23: Scheme of FSP.

2.2.1 FSP variables

FSP depends on technological parameters to achieve surface quality and flawless modified materials. These parameters can be divided into two groups, differentiating those which are machine dependent (torque, forces) from independent ones (WP, tool).

Since tool parameters have been deeply detailed in the previous chapter, this chapter focus on involved forces and loads. Forces generated when stirring the material can cause tool wear or deformation in clamping system. To acquire knowledge about how these phenomenon influence the expected result is crucial to predict, monitor and control them. Many measuring methods can be useful: direct measurement instruments like dynamometers, strain gauges or load cells, and indirect methods, such as monitoring power or current of the driver motor. Measures focused on drive motors are more affordable [45].

One measurement system developed by [46], works on the strain gauges technique allowing measurement of traverse and side forces at the same time. Usually, four strain gauges are disposed in the stirring machine to record the forces in two directions: parallel to the weld nugget and perpendicular to the WP (F_x and F_z). Also, with load cells inside the machine where can stay in contact with the tool and connected to a data acquisition systems is possible to measure local forces [47].

FSP may be performed using specialized or milling machines. First ones include measurement systems while second ones need an additional measurement head unit. These measurement units have four main elements: measuring unit where process forces and torques are recorded, a device to remove excess heat to protect the tool, tool needed for milling and the required software to capture and display data.

In order increase the chance to predict attributes of the final surfaces, process parameters equations and behavior should be identified:

$$(1) M_{total} = M_{shoulder} + M_{pin-bottom} + M_{pin-surface}$$

$$(2) Q_{total} = M_{total} \cdot \omega$$

where ω = rotational speed (rpm)

$$(3) Q_{total} = Q_1 + Q_2 + Q_3$$

With Q=heat generated at:

$$Q_1 = \text{under tool shoulder}$$

$$Q_2 = \text{pin surface}$$

$$Q_3 = \text{pin tip}$$

A study done by [48] published connections within parameters and forces. Increasing any of rotational speed, shoulder or pin diameter directly increases Fx force. Instead, increasing the traverse speed decreases Fx. It is important to oversee the travelling affected since small variations directly increase torque, vertical and traverse forces.

Regarding Fz, it is also influenced by the same parameters as Fx. However, the higher the travel speed, the higher Fz and the volume of stirred material. Rotational velocity increase carries a rise in temperature which softens more the material so Fz decreases.

About torque, next figure (Figure 24) shows how torque changes when varying rotational speed. More rotational speed leads to decrease torque as a result of a lower friction coefficient produced by the higher temperature [49]. Two zones appear during this phenomenon: primary and secondary, where the streamlines trend to concentrate.

Figure 25 shows that spindle torque is not significantly affected by travelling speed but is directly proportional. That increase might take place, in one hand, by lower material movement, and in the other hand by the reduction in convective cooling.

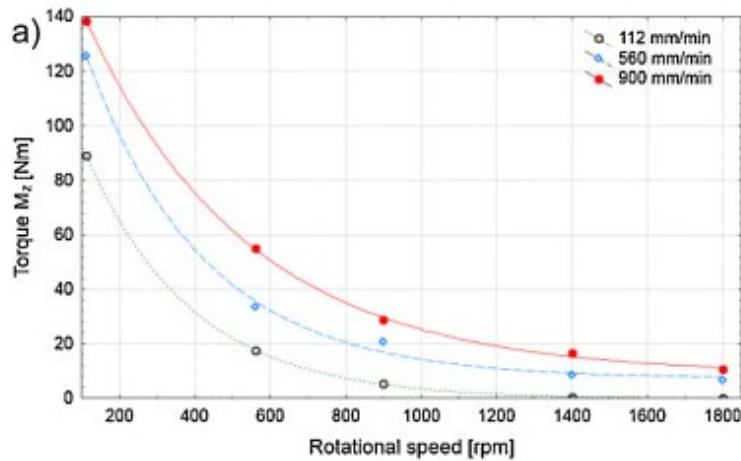


Figure 24: Influence of rotational speed vs torque, aluminum alloy AlSi6Cu4

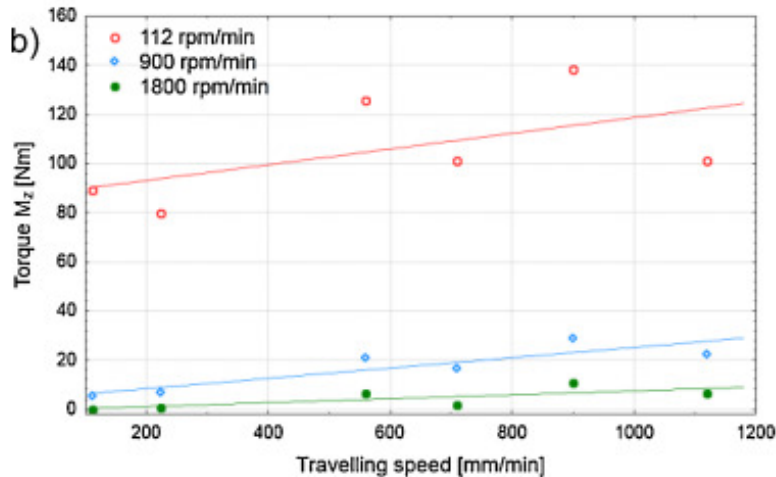


Figure 25: travelling speed vs torque, aluminum alloy AlSi6Cu4.

2.2.2 Microstructure

FSP aims to fine microstructure to enhance material mechanical properties. The strongest materials are those with fine grains structures and this will determine their final applications. These materials will probably find main applications when working under severe conditions, e.g. aeronautical, energy sector or biomedical applications [50].

Materials can be gathered in three divisions depending on the grain size: nanocrystalline ($d < 10^{-8}$ m), ultrafine grain (10^{-8} to 10^{-6} m) and traditional ($d > 10^{-6}$ m) [51]. The passage from one state to another is made by exerting extremely high strains to generate dislocations in the material to be later re-ordered and form a pattern of grain boundaries. In practice, achieve ultra-fine grain structures is limited due to two reasons. First, techniques employed produce cross sectional reductions of the WP limiting the number of total strains. Second, low workability of materials at room temperature impede to create ultra-fine structures with the strains inflicted by current techniques. Consequently, new processing techniques are required to get ultra-fine grain by means of severe plastic deformation (severe strains at low temperatures without any cross section reduction in samples). To cover these needs, severe plastic deformation techniques have been proposed, such as high pressure torsion, twist extrusion, multi directional forging and more, where undoubtedly the most outstanding is FSP.

In FSP, the factors determining final microstructure are responsible of different parts in microstructure refinement [26]:

- Chemical composition: determines available strengthening and influenced by temperature and strain.
- Temper conditions: preceding material is responsible of future effect during FSP, especially in HAZ.
- Process parameters: determine boundary conditions.
- Geometries: like tool shape, heat sinks or plate gauge determine temperature distribution.

Figure 26 shows the stages followed to produce microstructure refinement. The tool is tilted to increase the forging action. Since the rotating shoulder friction heats the WP and the pin moves the softened material, leading to a material flow, the process can be understood as hot deformation, where the dynamic recrystallization in charge of new grains origination is divided into three types:

1. Discontinuous dynamic recrystallization, due to nucleation of lately grains.
2. Continuous dynamic recrystallization (CDR): implies the formation of a variety of low angle boundaries to finally achieve grain development.
3. Geometric dynamic recrystallization: takes place when grains are greatly elongated because of critical hot deformation.

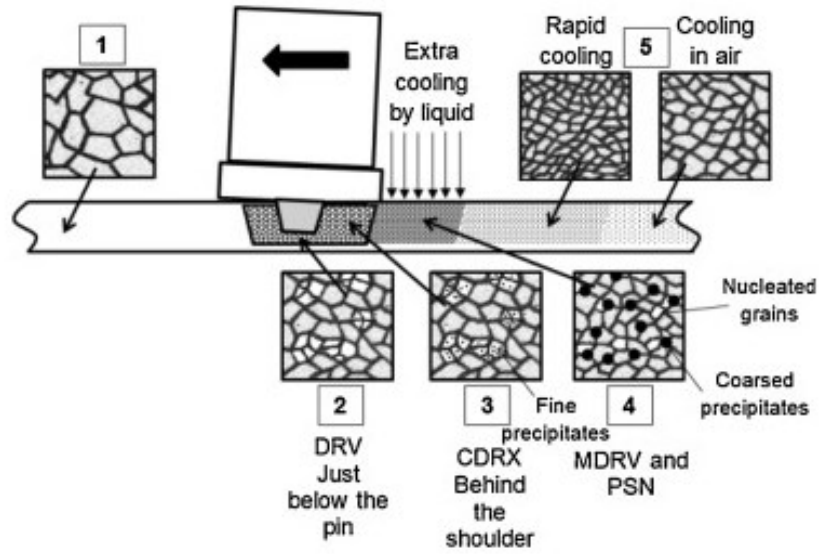


Figure 26: Microstructural evolution during FSP, aluminum alloy 5083.

During FSP, the temperature gradient brings solutes to precipitate. As consequence, when DRV is interfered by the precipitation particles starts a restoration mechanism which finishes in the occurrence of CDRX. CDRX restoration finishes in regular and fine grains. Figure 27 plots a FSP applied to an Al-Si alloy. Dark particles correspond to Si while Al phase looks bright. Also, shoulder region (top) and pin stir area (bottom) can be distinguished. The stirred region is composed of deformed material but to a lesser extent in the direction of RS and includes rotational shear material (RSM) slightly displaced to the advancing side. In RSM, Si particles are uniformly distributed between Al [52].

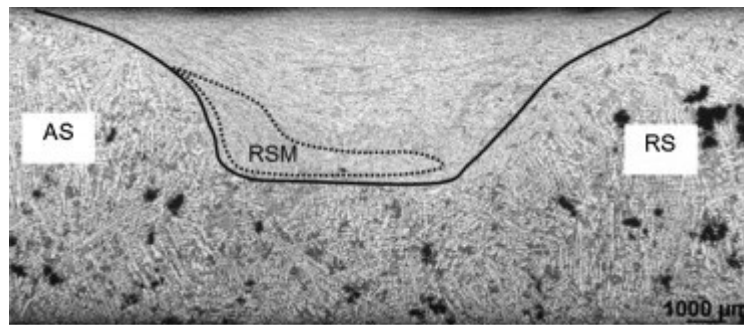


Figure 27: Al-Si section after FSP. Advancing side (AS), retreating side (RS) and rotational shear material (RSM).

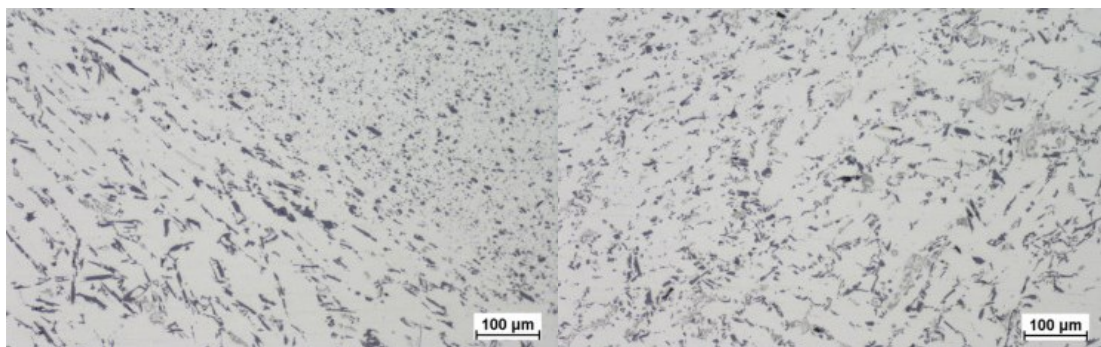


Figure 28: Microstructure of advancing (left) and retreating (right) sides of aluminum alloy after FSP with Triflute tool.

Extra cooling supply helps FSP to produce UFG materials. With a properly designed cooling system, the samples are quickly cooled increasing the reduction of grain size. One extended method is submerging the plate into liquid coolant. Furthermore, this helps to hinder the growth of recrystallized grains by cooling down the material right away behind the tool [53]. Some other methods are multipass techniques. As the number of passes increase, the grain size is progressively decreased. Changes are observed from the first pass, but it is not until the sixth when the changes are again significant.

2.3 Friction stir channeling

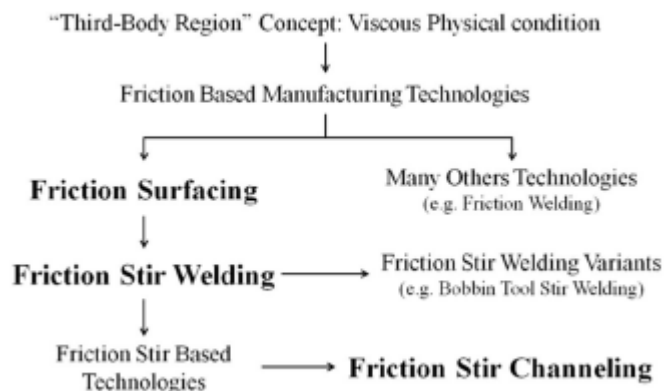


Figure 29: Technological interrelations of the linear friction based manufacturing technologies [4].

Friction stir channeling arose by chance. During FSW and FSP explained above, when the required parameters, such as processing conditions or tool geometry and features, are not properly selected some defects emerge on the weld zone. One of them, known as wormhole which is located at the base of the nugget [54], enables to reconvert a defect into a manufacturing technique for heat exchangers applications using the continuous inner channel formed. From that point, FSC aimed to discover the causes of the defect in order to produce good quality channels.

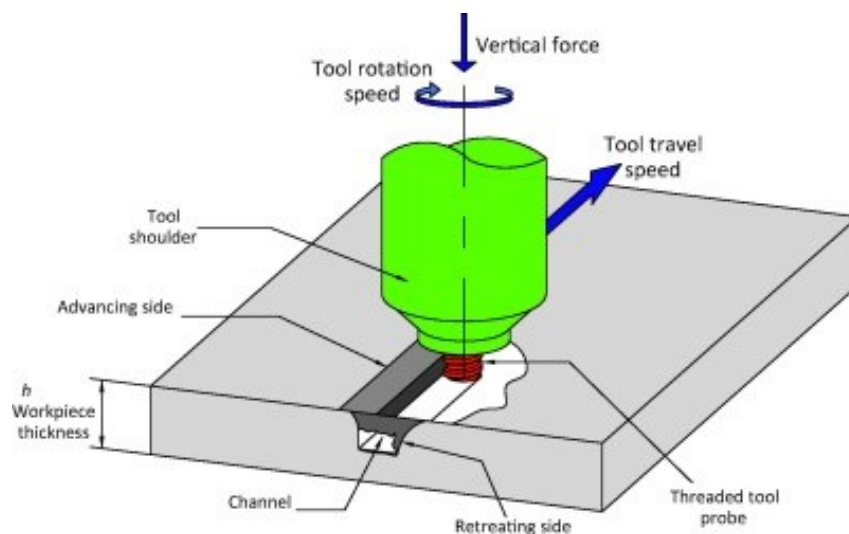


Figure 30: Schematic of friction stir channeling⁶.

⁶ Source: <https://www.sciencedirect.com/science/article/pii/S1350630715000564>

The patent carried out by Mishra [55] shows, for the first time, how this technique can create an endless hole in a single plate just by one step and choosing the appropriate processing conditions, including a material reverse flow. Main aspects to succeed in FSC are:

1. During rotation contoured tool should be able to guide the material flow upwards to the shoulder bottom face in contact with surface. For clockwise rotation, a right hand threaded tool is needed while a left hand threaded tool for counterclockwise rotation.
2. In order to let the surplus material removal, there is a clearance provided between the WP and the shoulder. There, the coming material from the base of the pin is placed. That is the main difference with FSW and FSP, where the shoulder is in contact with the WP surface to produce the necessary forging action to create flawless welds or processing.
3. The channel shape, integrity and size are controlled by the distance from the WP to the shoulder.

Figure 31 shows a cross-sectional image of a channel using FSC. The material from under the pin is taken away with a proper orientation of the threads on the pin and the tool rotation to be relegated into the clear area within the shoulder and WP. The amount of material deposited in the clearance area determines the channel area. The bigger the material removed, the greater the area. Instead, the shape depends on tool profile [54]. At the first attempts, channel shape was very irregular preventing area stability.

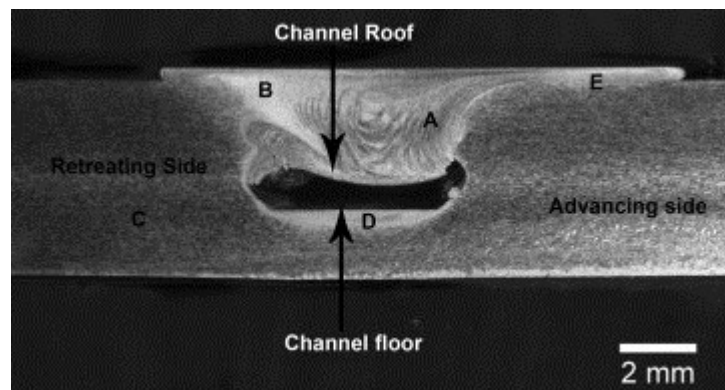


Figure 31: Different process regions of a channel: channel nugget (A-B), parent material (C), channel (D), material removed from channel nugget (E).

As in FSW and FSP, during FSC the plasticized region mutates and acquires new microstructure and properties. Despite the solid state process, there are three different patterns in the material flow that makes possible the channel formation. This phenomenon is known as the “*three body region concept*” [56]. For the case of aluminum alloys this region is characterized by nearly low flow stress and, thermically speaking, temperatures above recrystallization point but under melting point.

FSC mainly relies on heat generated from dissipation during material flow due to plastic deformation but also in the heat coming from friction (tool and WP), similar to heat produced during FSW. As the material comes closer to the fusion temperature, heat produced by friction dissipation tends to zero, so maximum temperature reached during process is limited by the fusion temperature, that’s why the deformation happens in solid state. It is impossible to suffer fusion when only plastic deformation is happening.

One of the disadvantages of FSC is the high roughness of the modified surface. The material ripped from the inside of the piece and moved beneath the shoulder alters surface's uniformity leaving an undesirable surface finish. Nevertheless, new developments carried out by P. Vilaça and C. Vidal allow different material flow [57]. A controlled material amount flows out from the WP producing the inner channel, but the plasticized material is not deposited in the processed surface. It is directed outside in the form of toe flash. The featured tool enables this flow move to the periphery of processed zone from the bottom of the shoulder. So, while the channel is produced, process surface still with same level and finish as it had before processing. Unlike what proposed by Balasubramanian et al. [54], who remarked the importance of the gap between shoulder and WP, this developed tool do not need initial clearance, depositing the material in the sides and back of the shoulder. Also, main process parameters can be recalculated to control size, shape and integrity of the channels.

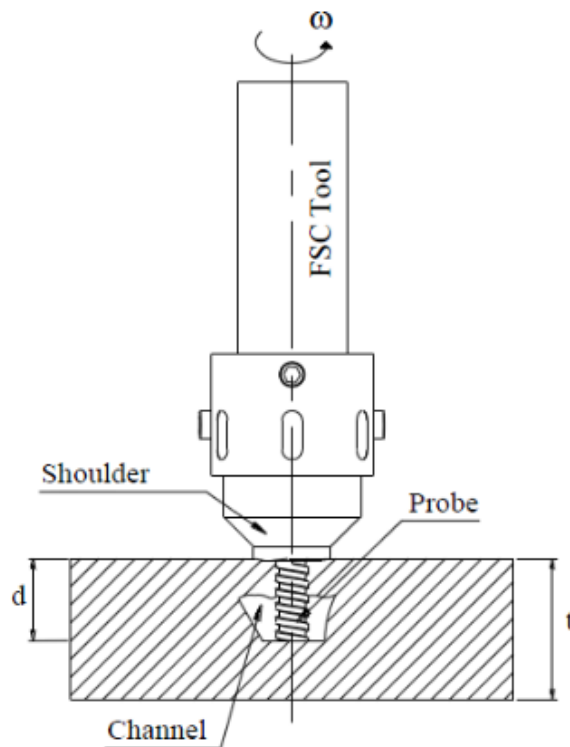


Figure 32: Schematic of FSC new process [57].

2.3.1 Channel formation

To understand the channel formation during FSC is essential to analyze the zones generated during the process. In Figure 33, the work presented by Vidal et al. [58], shows the different material flow path and the microstructural regions once the tool has passed over. Looking at it, there are several distinguishable zones. In the middle there is the weld nugget, with the stirred zone in the upper part (limits defined in dark grey) while the channel remains in the bottom. The base material (zona A and bottom of the piece) is the unprocessed parent material, so preserves its original properties. The channel disposition suggests the orientation of the tool threads and direction of the tool rotation. The plasticized material is moved upwards and then pushed outwards to be deposited in the advancing side proximities, which is the side where the travel direction has the same direction as the velocity vector in the tool rotation. So, this tool movement is counterclockwise rotation

and travel direction outside from the plane of the figure. TMAZ region collects a low concentration of grain refinement, mainly located at the stirred zone.

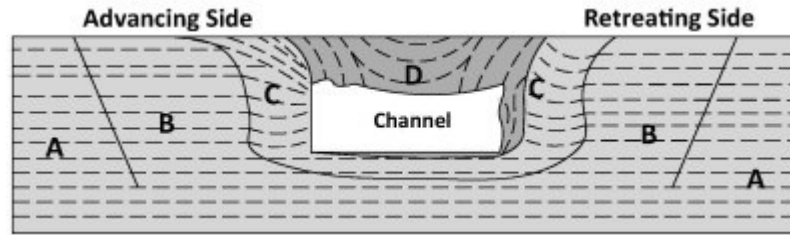


Figure 33: Microstructural regions after FSC: base material (A), HAZ (B), TMAZ (C), stirred zone (D) and channel [58].

In the FSC model of Balasubramanian the pulled upward material is deposited in the gap resulting in an accumulation of material under the shoulder, but none downward force assists the pull and the amount of material pulled is notably less. One of the benefits provided by the tool in Figure 32, developed by P. Vilaça et al. is that the process of withdrawing the material is aided by a vertical descending forging force which creates extra pressure on the WN helping the channel to get compacted and intensifying material flow. This upgrade explains having no clearance between WP and shoulder. Also, the scrolls aid to push outwards the stirred material [59].

None of the versions are defect free. The defects are slightly different but move in the same direction. For Balasubramanian initial version, two types are detected: discontinuous channels created when extremely cold processing conditions and insufficient material extraction to till the shoulder-WP clearance, so the shoulder is unable to distribute the material not closing the processed zone. Similar situation happens with the newest version. With cold conditions there is easier for open channels to appear but, as said, the more material moved by this version almost always avoids open channel appearance. On the other side, with hotter conditions most probably is the probe breakage. C. Vidal and P. Vilaça defined the specific parameters to optimize the process, although still conditions that might cause open channels: tool travel speed, shoulder pressure and base material [59].

2.3.2 Channel shape

First FSC technique produced channels similar to an ellipse. Slightly variations on the process parameters produce nonlinearly changes in the shape. The term “*heat index (ratio of the square of the tool rotational rate to the tool traverse speed)*” is used to differentiate the variated process parameters [60]. This index helps in determining the stress conditions suffered by the probe and WP. For a high heat index, there is a lofty volume of material extracted because of a low traverse speed, or the high tool rotation rate. Shape and finish of the side walls, including roughness, depend on the pin features.

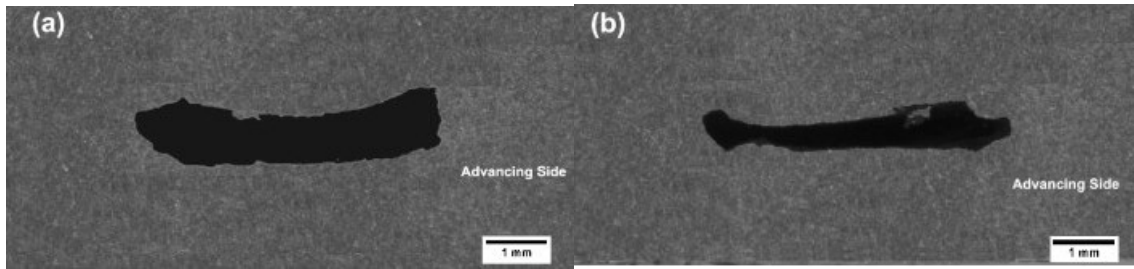


Figure 34: Different shapes at: 1100 rpm, 2.11 mm/s (a) and 1100 rpm, 2.96 mm/s (b).

Unlike Balasubramanian et al. work, when a downward forging force applied on the surface by the shoulder the main disadvantage of FSC is solved. This force enables to have greater channels with lower heat indexes, allowing less hard conditions for the tool and also longer continuous channels. As a result, the channel shape changes from an oval shape to look more like a trapezoid and do not suffer important variations when varying process parameters.

The experiment carried out by P. Vilaça et al. [61] utilized four different conditions to analyze the shape. Channel shape can be attributed to the amount of processed material displaced from the base of the pin in each rotation and also to the compacting force exerted by the shoulder on the ceiling of the channel. Although conditions A and D have similar heat indexes, the ceiling in D is very irregular due to an excessive amount of frictional heat and excessive softening of the material, perhaps because of high rotation and travel speeds. Meanwhile, the least defined shape takes place for the lower heat index, condition B. Nevertheless, it can be seen that channel shape has small variations compared to the variations induced in processing conditions.

FSC Condition	Tool rotation speed (rpm)	Tool travel speed (mm/min)	Heat Index (rpm ² /(mm/min))
A	600	80	4500
B	600	150	2400
C	800	80	8000
D	800	150	4266.7

Table 2: FSC process parameters [61].

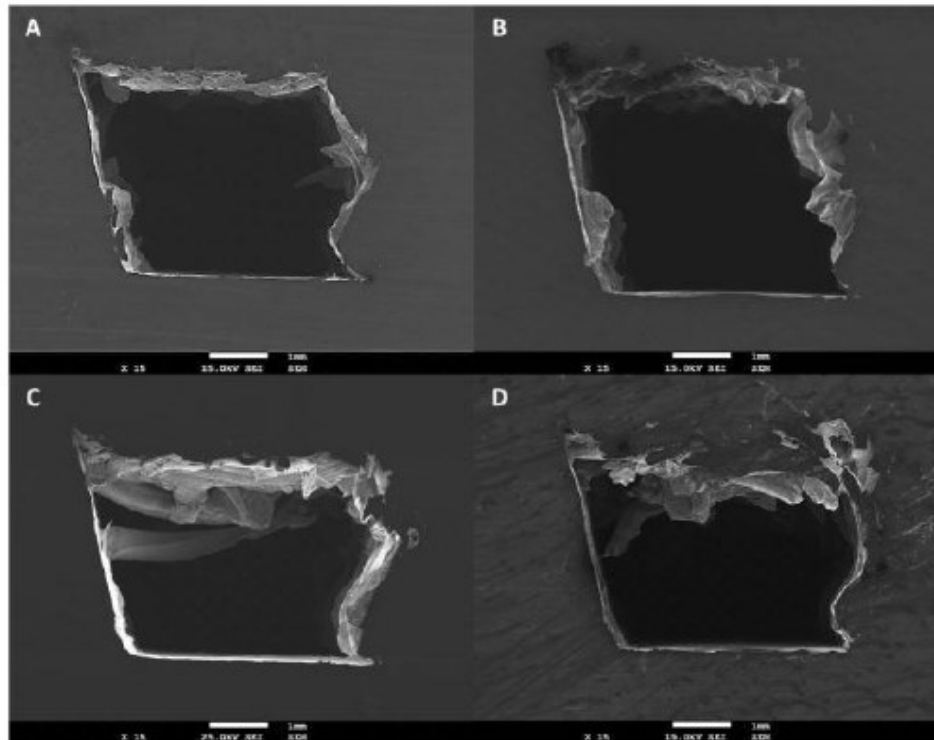


Figure 35: Channel geometries produced with different FSC processing parameters, corresponding to Table 2.

To standardize and determine possible trends, two characteristics were determined: closing layer thickness (D) and shear angle (α). The results establish that as the closing layer thickness decreases, the channel area increases. Nonetheless, shear angle has no direct relation with the values of channel shape.

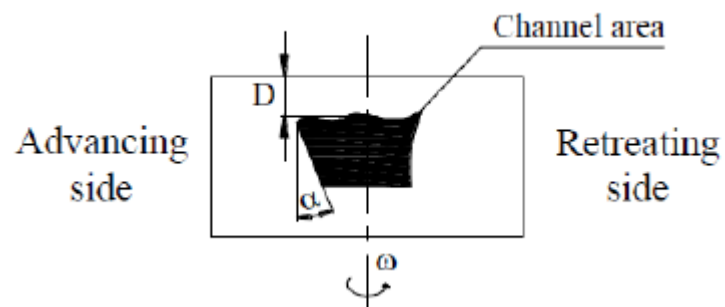


Figure 36: Schematic of a channel with parameters D (closing layer thickness) and α (shear angle).

2.3.3 Channel size

As described in the work of Balasubramanian et al. channel size is based on the next principle: “for any tool, the maximum possible channel area is the maximum volume of material that can be displaced by the probe at any given instance, over a unit length” [54]. Thus, for a specific plunge depth, a channel with the greatest area is expected to be produced by the tool with the highest surface area of the probe.

To demonstrate this principle, several experiments were carried out. The one done by Balasubramanian et al. [54] established a direct relationship between the channel area and two process parameters: tool rotation rate and traverse speed:

$$\text{Area} = K * (\text{rotational rate})^\alpha * (\text{tool traverse speed})^\beta$$

With K , α and β values determined by least squares method

After the coefficients were determined, obtaining a negative value for α while a positive value for β , the results for FSC with 2 different plunge depths were plotted (Figure 37). Analyzing the figure is noted that there is a high range where the channels created are continuous, stable and defect free. Open channels are observed when inadequate operating conditions. Extremely cold conditions lead to an inappropriate material flow to the clearance therefore there is a leak of material for the shoulder to fill the top of the channel. Increasing the tool traverse speed. In the optimal zone, increasing traverse speed or decreasing rotational rate generates higher channel areas.

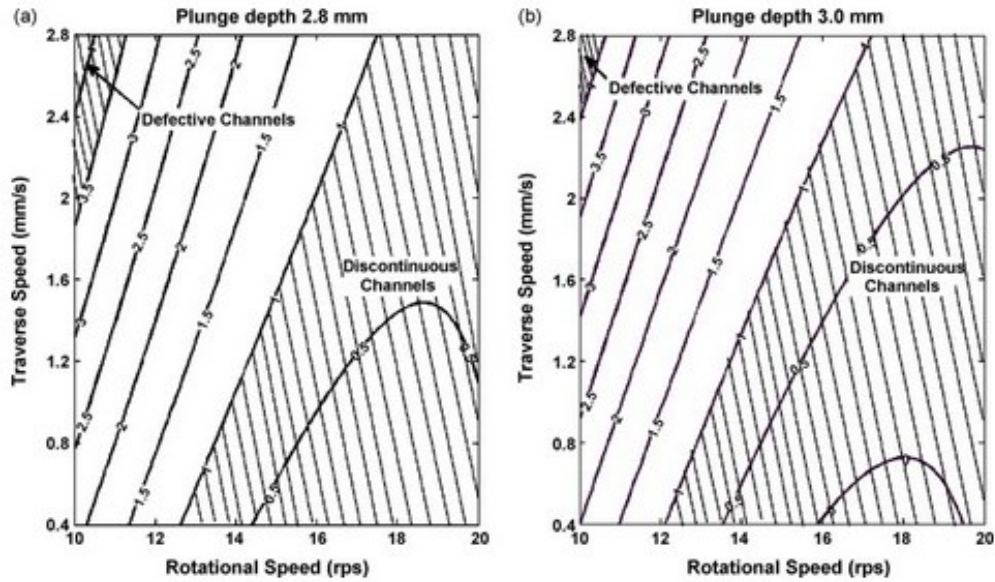


Figure 37: Variation of the channel area depending on traverse and rotational speeds for two different plunge depths.

Following the same procedure, P. Vilaça et al. experimented with four different conditions depending on the modification of two key parameters: tool rotation and travel speed. Table 3 collects the results of the experiment. For same rotation speed, the higher area was achieved for a bigger tool traverse speed. In the other hand, for same tool travel speed, lower rotation speeds perform higher channel areas. Comparing the channel size of these two techniques, it is remarkable that thanks to the upgrading in the Vilaça's tool the channel areas are bigger in size, about a 330% [59], broaden the range of services it could be used to and maximizing its potential.

FSC Condition	A (mm ²)	Tool rotation speed (rpm)	Tool travel speed (mm/min)
A	13.49	600	80
B	14.01	600	150
C	12.75	800	80
D	12.88	800	150

Table 3: FSC channel areas for different conditions [61].

2.3.4 Surface roughness

The surface roughness on the inner surface of the channels highly affects fluid flow behavior, since the variations in pressure drops depend on roughness pattern and dimensions.

By means of cross sections of channels, Balasubramanian demonstrated different surface properties produced depending on several parameters. These properties vary prominently at the upper and lower surfaces. The bottom of the channel is usually flat and smooth thanks to the nature of the pin base, while the ceiling used to be rough and wave, where the roughness point is in the orientation of the travel direction. The study made by Balasubramanian [54] determined the existing concordance of the material displaced in each rotation and the distance between consecutive peaks in the surface roughness. In Figure 38 the distance between peaks is 0.107 mm made by a tool pitch of 0.106 mm/rotation.

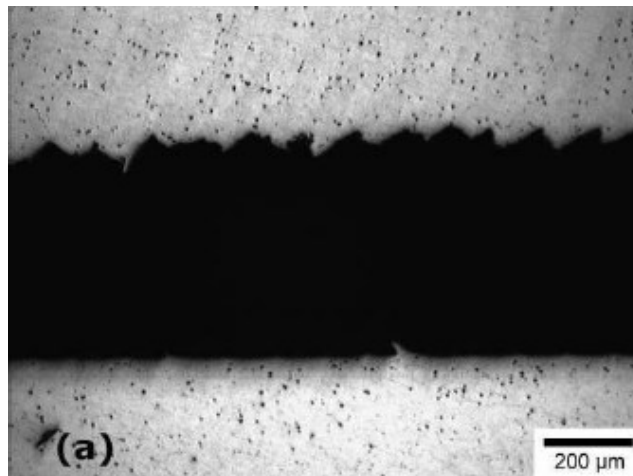


Figure 38: Cross section of a FSC work piece showing the roughness of the channel [54].

Regarding the channel side walls, there is also discordance between the advancing and retreating side. The roughness in the advancing side of the channel is insignificant compared to retreating side. This is due to the tool rotation, displacing the material from AS and leaving it on the RS with a low surface finish, increasing the pressure drop along the channel and accordingly enhancing heat transfer to the liquid (when used as a heat exchanger). AS presents a surface very similar to the bottom of the channel [62].

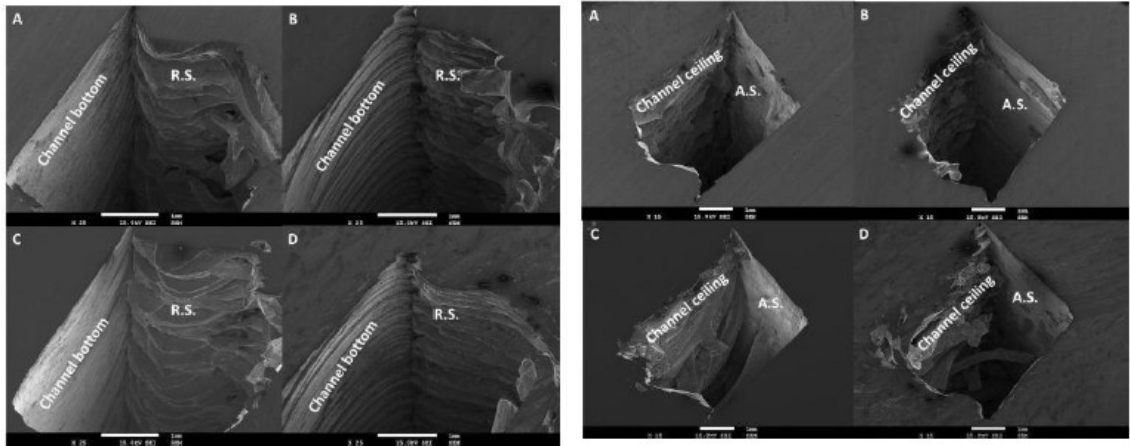


Figure 39: Roughness at side walls, bottom and ceiling of FSC by four different processing parameters [62].

2.3.5 Hybrid friction stir channeling

Based on the same principles as the methods explained before and considered as a development from FSC, Hybrid Friction Stir Channeling (HFSC) consists in a new technique to manufacture internal closed channels which also adds a weld joint between various elements. Both internal channel and weld joint are made in a single step by a simultaneous action, combining the advantages of FSW and FSC in a stable process. The proper design of the tool and working parameters make the process controllable and repeatable. The range of channel dimensions achieved by HFSC is very wide. Channels are characterized by constant cross section and internal roughness which increases the surface area and creates turbulent flow even when low flow speeds. Combining both turbulent flow and higher surface area improves heat transfer to the cooling liquid, making HFSC suitable for the production of heat exchangers for thermal management [63].

To weld and join both pieces, the non-consumable tool employed must be in contact with both materials as shown in Figure 40. Six different regions describe the tool: (1) tool geometrical features (2) shoulder (3) probe in contact with secondary material by a downward force to create the weld (4) channel section (5) shoulder features to push down the weld material and push out (6) the flash to seal the channel.

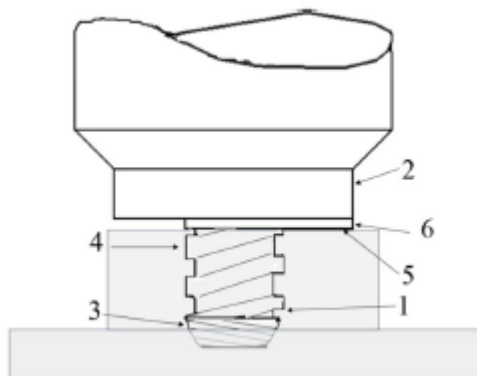


Figure 40: HFSC tool and contact region.

HFSC picks the benefits from FSW to weld in solid state two different materials and FSC manufacturing internal closed channels. The simplicity with which it is manufactured and its application to several materials give great flexibility for any requirements. Main application for HFSC manufacturing is thermal management. Heat exchangers manufactured by HFSC offer a wide variety of advantages faced to other current techniques. The broad range of channel paths with internal roughness and the save on material costs are an example of them. Also, the thermal bridge generated when welding both materials leads to an improvement in heat transfer to the coolant and so achieve lower maximum temperatures.



Figure 41: Cross section detail of HFSC application.

The prototypes used in the department and possible future validations are machined on an ESAB LEGIO 5UT machine (Figure 42). It is designed for FSW using a hard framework for high performance tasks. The spindle head is powered using an AC engine and is attached to a cart providing movement in X and Y axis. For the Z movement, a hydraulic cylinder exerts up to 100 kN of force. Working range is 2000 x 400 x 200 (X, Y, Z axis) and tilt angle can be set up to a maximum of 5° around the Y axis. AN external liquid cooler provides refrigeration to the spindle head and FSP tool. The process is monitored using the control panel which shows position, forces, speed or spindle torque and it's also used to adjust processing parameters [63].

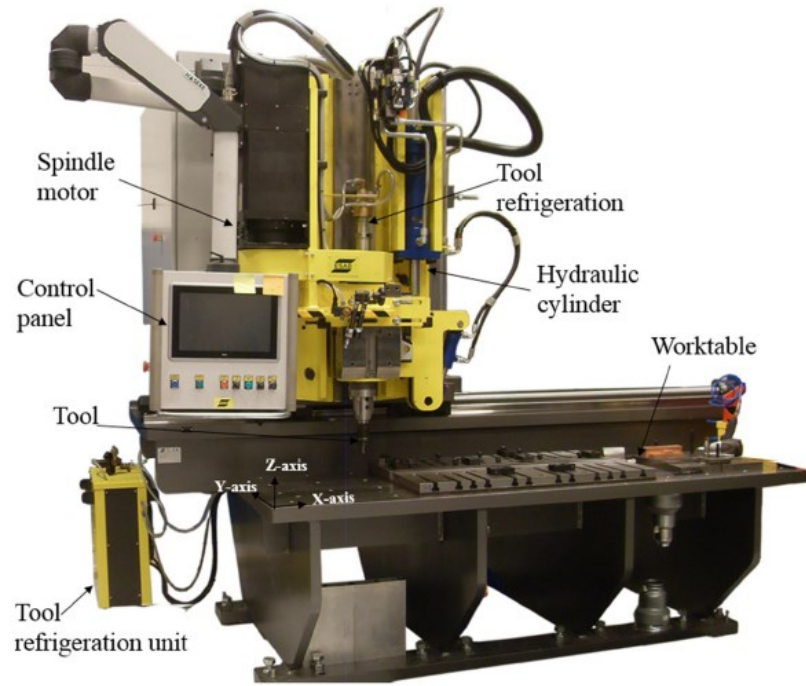


Figure 42: ESAB LEGIO FSW 5UT [63].

2.3.5.1 Thermal contact resistance

The main issue to deal with when heat transfer between two materials in contact is the thermal resistance created in the interface. Of course, there is no continuity of the material properties throughout the joint and so appear new conditions which redefine the model.

Thermal contact resistance is the thermal conductivity of the new interface and depends on several factors, such as material properties, surface roughness interface pressure and interface temperature (Table 4). Typically, it is calculated by measuring the heat flux and temperature variation across the interface. However, since pressure also affects the resistance, it is important to keep the material themselves with a constant load so the pressure in the interface does not vary. Either way, characterization of thermal contact resistance can be difficult because the load distribution is not uniform along any surface.

Factors influencing thermal contact resistance

Surface micro and macro topography (asperity roughness, surface waviness)
Surface micro hardness
Solid thermal conductivities
Cleaning, oxide and coatings in surfaces
Substance nature in interstitial gap
Contact pressure
Gap thickness
Gas pressure if gas in the interstitial gap
Temperature of the surfaces

Table 4: Factors influencing thermal contact resistance.

When getting in touch two metallic materials by a pressure applied to each other, only a little fraction (about 2%) of the whole surface area is in contact due to the unavoidable

non-flatness and roughness of every existent surface. Roughness and waviness inherent to any surface are imperfections consequent of tool shape, machining processes or heat treatments. The small points in which the surfaces are in contact make the pressure greater than apparent in contact region. As the pressure applied increases, the highest surface asperities get deformed creating wider regions where the heat flux can flow by conduction. None surface behaves as an ideal one and the thickness of the joint can vary from 0.5 to 60 μm . As seen in Figure 43, if there is a heat flux across a contact interface the heat flow is restricted to conduction straight through the contact spots, which finally results in a much smaller contact area than the apparent one. That restriction in contact area makes the heat difficult to flow, causing the thermal resistance [64].

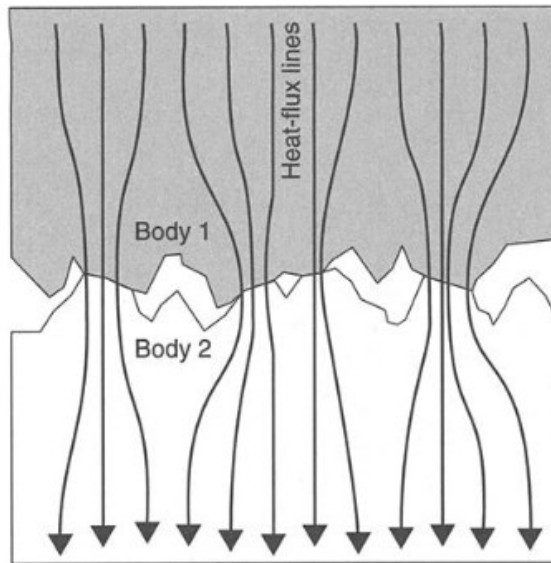


Figure 43: Microscopic view of two materials in contact.

Rarely, this contact is produced in vacuum conditions. Thus, the presence of any fluid or solid in the gap within both surfaces may contribute to facilitate or restrict the heat transfer at the interstitial medium, depending on thickness, thermal conductivity and hardness of that medium.

Next equation defines the contact resistance at the junction defined by the temperature difference in contact surfaces:

$$\frac{1}{S * \alpha_c} = \frac{T_1 - T_2}{\dot{Q}} = \frac{\Delta T}{\dot{Q}} \quad \text{or}$$

$$\frac{1}{\alpha_c} = \frac{T_1 - T_2}{\dot{q}} = \frac{\Delta T}{\dot{q}}$$

Where:

T_1 and T_2 \rightarrow temperature of the bounding contact surfaces

S \rightarrow area across the heat is transferred

α_c \rightarrow heat transfer coefficient for the junction, thermal resistance

Some simplifications are necessary to develop analytic models. Next assumptions are made for the contact resistance models:

- Isotropic thermal and physical properties for contacting solids.
- Solids in contact are thick compared to their surface roughness or waviness.
- No vibration effect present, static contact.

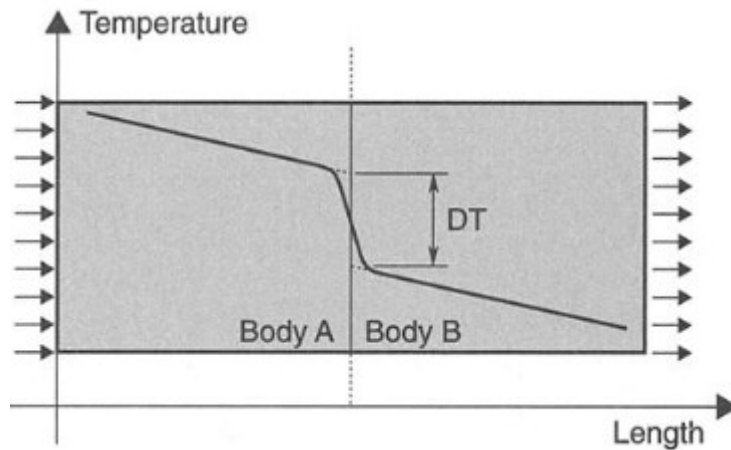


Figure 44: Temperature drop in the joint [65].

Determine the contact resistance between aluminum and copper, which are the materials used in our study, might be difficult by our available sources. Fortunately, William Edward Stewart Jr. [66] carried out a field study on thermal contact resistance between metals. A part of the study focused on the contact copper-aluminum using circular cylindrical specimens with flat and polished contact surfaces to a roughness of approximately 2 micro inches. Loads were applied from 20.7 to 124.2 psi. In general terms, it was demonstrated that thermal contact resistance decreased with increasing load and decreased when increasing time after initial loading.

The contact resistance is lower for a heat flow from materials of higher thermal conductivity to materials of lower thermal conductivity. From Figure 45, the desired value comes from the heat flow copper to aluminum. Depending on the interface pressure, the value ranges from $7.83 \cdot 10^{-4}$ to $9.19 \cdot 10^{-4}$ Hr*Ft²*F/BTU. As an approximation, during simulations it was used an average value of $8.5 \cdot 10^{-4}$ Hr*Ft²*F/BTU.

In the studies explained later, the value of thermal resistance was set in the SI units, with corresponds to:

$$8.5 \cdot 10^{-4} \frac{\text{Hr} * \text{Ft}^2 * \text{F}}{\text{BTU}} = 1176.47 \frac{\text{BTU}}{\text{Hr} * \text{Ft}^2 * \text{F}} = 6677.64 \frac{\text{W}}{\text{m}^2 * \text{K}}$$

In the knowledge that this value is taken from literature and could not be accurate since depending on several factors, the fictional material was defined with this thermal conductivity value once it was multiplied by the thickness of the layer. Estimation of thickness from interstitial material could seem to be high given that it simulates a gap between to surfaces in contact. Nevertheless, it is just enough to observe influence in temperature conduction.

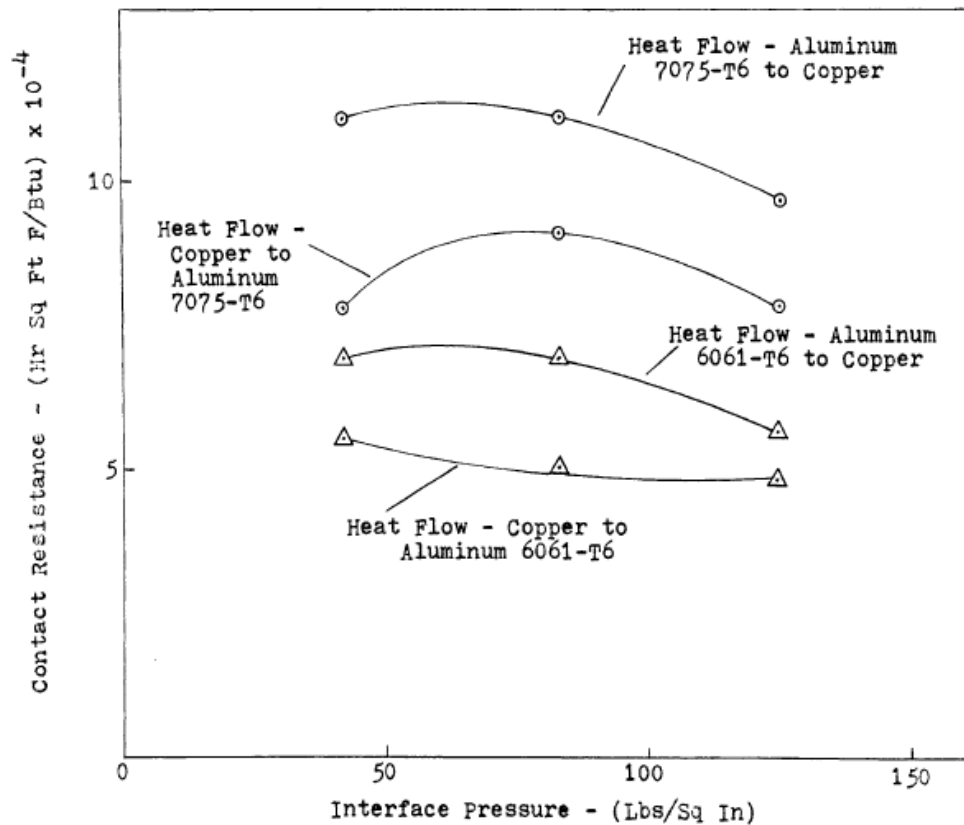


Figure 45: Thermal contact resistance for aluminum 7075-T6 and copper [66].

3 Model and solver theory

Computational fluid dynamics software are used around the world in many domains. ANSYS develops, markets and supports engineering through simulation software to predict how a certain product will work and react under a real environment. Fluent is a finite volume method which manages mesh elements as control volumes. In the center of each element, the governing equations are calculated, so the fluxes across the element faces is maintained. Basically, the information that goes inside the cell must exit through other faces or be filed. The results are converted into integral surfaces, known as face fluxes, repeating the process iteratively up until there is convergence in the solution for all the elements.

Fluent software is divided into three main tools called modules:

1. Pre-processor: deals with the creation of geometry and mesh, defining solids and fluids. It is provided with a graphical interface.
2. Solver: this finite element processor includes the analysis of heat transfer and fluid dynamics. Here, the governing equations are solved.
3. Post-processor: also provided with a graphical interface, shows the solution by means of charts, contours or plots.

In order to improve the results by the available power of the current PC, double precision variables and serial processing were used on the simulations. Despite a higher usage of the memory, the double precision variables allow saving more data per cell to be later entered in the solver and reducing the truncation errors characteristic of single precision variables in those areas where the gradients are great. Parallel processing increases too

much the memory needs and its worth to assume larger times to solve the equations using the serial processing because of the low memory capacity.

To solve the governing equations segregated method was chosen since the computing power was limited and this method is simpler and less computationally exhaustive.

3.1 Governing equations

For the required case, the primary conservation equations solved by Fluent for the absolute velocity formulation and a steady and turbulent fluid flow with heat transfer are [67]:

$$\text{Mass conservation} \rightarrow \frac{\partial \rho}{\partial t} + \nabla \cdot \rho \vec{v}_r = 0 \quad (1)$$

$$\text{Momentum} \rightarrow \frac{\partial}{\partial t} \rho \vec{v} + \nabla \cdot (\rho \vec{v}_r \vec{v}) + \rho(\vec{\omega} \times \vec{v}) = -\nabla p + \nabla \bar{\tau} + \vec{F} \quad (2)$$

$$\text{Energy} \rightarrow \frac{\partial}{\partial t} \rho E + \nabla \cdot (\rho \vec{v}_r H + \rho \vec{u}_r) = \nabla \cdot (k \nabla T + \nabla \bar{\tau} \cdot \vec{v}) + S_h \quad (3)$$

Where:

$$\begin{aligned} \vec{v} &= \text{velocity vector} \quad ; \quad P = \text{pressure vector} \quad ; \quad \rho = \text{density} \\ E &= \text{enthalpy} \quad ; \quad T = \text{temperature (K)} \end{aligned}$$

The expected turbulent flow is modelled by the RNG-based k-ε turbulence model, derived from Navier-Stokes equations. Next equations are used in the simulations to obtain kinetic energy, turbulence, dissipation and the k rate dissipation [67]:

$$\frac{\partial}{\partial t} (\rho k) + \frac{\partial}{\partial x_i} (\rho k u_i) = \frac{\partial}{\partial x_i} \left(\alpha_k \mu_{eff} \frac{\partial k}{\partial x_j} \right) + G_k + G_b - \rho \varepsilon - Y_M + S_k \quad (4)$$

$$\frac{\partial}{\partial t} (\rho \varepsilon) + \frac{\partial}{\partial x_i} (\rho \varepsilon u_i) = \frac{\partial}{\partial x_i} \left(\alpha_\varepsilon \mu_{eff} \frac{\partial \varepsilon}{\partial x_j} \right) + C_{1\varepsilon} \frac{\varepsilon}{k} (G_k + C_{3\varepsilon} G_b) - C_{2\varepsilon} \rho \frac{\varepsilon^2}{k} - R_\varepsilon + S_\varepsilon \quad (5)$$

Equations solving is monitored seeking for the convergence of the equations which determine steady state. Further information about model equations and formulations to be seen in ANSYS Fluent guide [67].

3.2 Materials

For the different models studied, the main materials in which the geometries are manufactured are copper for the base plate and aluminum as support for the channels. As refrigerant, several fluids where used: water liquid, OptiCool and air. To define the governing equation, some material characteristics needed to be defined such as density, specific heat, viscosity and thermal conductivity. All data was taken at ambient temperature of 20 C. OptiCool properties were consulted into official DSI Venture website [68] at a given temperature of 40 C since it's the closest to the operating point. All parameters were

considered constant since they have a small effect on the simulation during the heat transfer and simplifies calculations. Next tables summarize the properties for both solid and fluid materials:

Fluid	Density (ρ) (kg/m ³)	Specific Heat (c_p) (J/kg*K)	Thermal Conductivity (k) (W/m*K)	Viscosity (ϑ) (kg/m-s)
Air	1.225	1006.43	0.0242	1.7894e-5
OptiCool	831	2203	0.1372	0.011841
Water	998	4182	0.6	0.001003

Table 5: Liquid cooling properties [69].

Solid	Density (ρ) (kg/m ³)	Specific Heat (c_p) (J/kg*K)	Thermal Conductivity (k) (W/m*K)	Thermal effusivity (e)(Ws ^{1/2} /m ² K)
Copper	8960	385	401	36983
Union	1	-	33.3	-
Aluminum	2700	900	202	22155

Table 6: Solid material properties [69].

The fact of having two different materials in the structure resides on their properties. Copper is chosen because of its high thermal conductivity which allows an efficient heat transfer from the batteries to the aluminum. Their thermal properties achieve uniform heat distribution on the surface in a short time and heat is easily dissipated. However, an entire structure built in copper would not be feasible due to the final cost (copper is much expensive than aluminum) and the extremely high weight (copper density is 3.3 times higher than aluminum). Thus, aluminum is chosen to build the majority of the structure. Also, the thermal junction within copper and aluminum and the lower thermal effusivity (measure of a material ability to exchange thermal energy with its surroundings) of the second one creates a smooth heat flow from the batteries to the water. Concerning the liquid coolers, their different properties are later studied to set their suitability to be used in the prototypes.

3.3 *Boundary conditions*

The boundary conditions can drastically affect the final solution. They can be defined on inlets, outlets and walls. Although most of the boundary conditions remain constant, several BC were tested to find out the most appropriate to optimize the heat removal. Since each model was designed for different purpose the BC slightly change.

- Inlet: set as velocity inlet, with 1 m/s and 288 K for all cases.
- Outlet: defined as pressure outlet at atmospheric pressure.
- Heat flux: heat inserted to the system, 5000 W/m² for every model, applied on the copper bottom surface. This value is an oversized approximation for a heat coming from power electronics.
- Walls: working on the worst scenario, all faces in contact with ambient air were set as adiabatic walls, so there is no convection through the walls and temperatures achieved are the highest possible ones. However, in the inner walls of aluminum forming the channel, in contact with the liquid coolant, also is possible to define the roughness, which value will change depending on the case of study. The equivalent sand grain roughness height to be set into the systems was calculated by:

$$\varepsilon = 3.1 * R_{RMS}$$

Where: $\varepsilon \rightarrow$ equivalent roughness height

$R_{RMS} \rightarrow$ Root Mean Square value of roughness height

- Interface: walls in contact with other bodies were automatically defined by the program as interface.
- Residuals: less than $1e^{-4}$ error to reach convergence for continuity, velocities, k and epsilon values. More restricting value for the energy, $1e^{-6}$.
- Model: energy equation ON, viscous, realizable k-epsilon, Scalable wall function. Computed for all zones.
- Solution methods: second order for pressure. Second order upwind for momentum, turbulent kinetic energy, turbulent dissipation rate and energy.
- Initial conditions: room temperature on every surface, 288 K for coolant inlet.

4 Cases of study

The study consists in carrying out a deep and complete evaluation of a simple HFSC geometry to extract all the available information to understand the behavior of the HFSC into different conditions and then be able to extrapolate all relevant data to more complex geometries and shapes. These cases of study serve as a base to acknowledge the parameters which influence the most in the performance of the heat exchanger and how their variation affect the rest of the parameters and final result.

To start with, the simplified model was chosen since the goal is not to simulate a real prototype, but just to understand the HFSC advantages and disadvantages. Because of this, it is enough with a simple geometry which allows carrying out several simulations in a short time, putting aside the typical issues implied in complex geometries or fluxes. The idea is to avoid a great amount of contacts, possible reverse flows and boundary conditions that will finally slow down the simulation.

Every model is divided into three main bodies: copper plate, aluminum and liquid coolant. In simplified models, length of the bodies is reduced in order to decrease the material costs in a possible future validation of the model. For the study, a new fictitious material has been added in the interface between copper and aluminum. As primary coolant, water is chosen due to its availability and abundance. Also, its high thermal capacity makes water an excellent liquid coolant. OptiCool and air were tested during simulations to analyze alternatives in the current market.

4.1 Calibration with no weld case study

The objective of this model was to represent the existing thermal gap in the contact between two surfaces. Heat transfer suffers from a barrier when moving between different bodies. Roughness and waviness characterizing any surface create gaps and peaks thus heat transfer method (conduction or convection) will depend on the path followed (see Thermal contact resistance 2.3.5.1). The thermal gap isolates the copper increasing final temperature. Gaps existing in the interface were unified and represented as a continuous layer between copper and aluminum surfaces made of a material with thermal properties imitating thermal conductivity of the interface copper-aluminum checked in literature [66]. Water was used as a refrigerant for the whole study of the model.

4.2 ***Calibration with weld case study***

HFSC creates a weld zone by the stirred material. This region properties are difficult to determine since it is a mixture of both materials involved in the welding. The percentage of each material that makes up the weld depend on probe depth, rotation speed and materials welded. Although it is not possible to accurately determine the composition, it is guaranteed the better thermal properties of the junction compared with a simple face contact. Thus, this case of study focused on the importance in having a thermal bridge to aid heat transfer. Same procedure as with no weld case study was followed: a layer of solid material simulating the thermal contact resistance copper-aluminum through the whole surfaces excluding the region under the channel, were the HFSC tool joins both materials by the weld. Geometry and detailed pictures are later shown.

4.3 ***Battery plate model***

First prototype goal was to cool down a set of batteries for electric vehicle. Heat flux enters the system by the top surface from copper plate. Prototype was designed to cover the maximum available surface without exceeding exchanger's weight. Knowledge acquired on calibration models were applied for a better convergence of the solution and accurate results. There are four independent inlets and their respective outlets to, if necessary, manage each source with different boundary conditions (if heat distribution varies non- uniformly in the surface, alternative inlet velocities can be settled in each domain). Prototype's purpose is to cool down batteries to work close to the range of optimal temperatures. Maximum temperatures allowed of 50 Celsius.

4.4 ***Network system model***

Designed for power electronics cooling. The complex shape (4.4) is due to specifications from the customer to fit in an established location. Power electronics position on the copper plate determines channel shape. The path must cover critical regions under the components. Pressure is an important issue to protect the components in case of failure. Bodies which are not part of the heat exchanger have been removed. Maximum temperature allowed for the power electronics is 30 degrees over ambient temperature.

5 **Fluid-dynamic modeling and analysis**

The goal of the fluid-dynamic simulation for the different cases of study was to acquire an idea of the suitability and performance of the heat removal by the geometries taking into account different boundary conditions and specifications given by the partner companies, aiming to obtain the temperature profile in the bodies during operation and look for the optimal shape for the channel and the exchanger.

The software chosen for simulation of heat transfer and fluid flow was Fluent computational fluid dynamics (CFD), developed by ANSYS. The mesh, geometry and boundary conditions for each model were defined and the results were examined by Fluent post-processing tools.

5.1 Geometry and mesh

5.1.1 Models A and B

Several geometries were used to study the influence of the parameters involved in the efficiency of heat transfer. The models were created aiming to simplify the calculations and clarify the appointment of boundary conditions. Main parts are basically the same leaving the minor changes to the interface. Aluminum and copper have same length and width: 0.4 meters and 0.06 meters respectively. The rectangular channel is located at the middle point of aluminum width, remains with same dimensions ($0.009 \times 0.004 \text{ m}^2$) and its lower edge is 0.001 meters far from the interface. However, model B has a small feature to represent the weld zone. It is a step which goes through the interface to contact copper surface. This is meant to represent the coupled material region produced when HFSC, so there is no interface but a continuous heat flow by conduction. Next tables sum up the dimensions for each model:

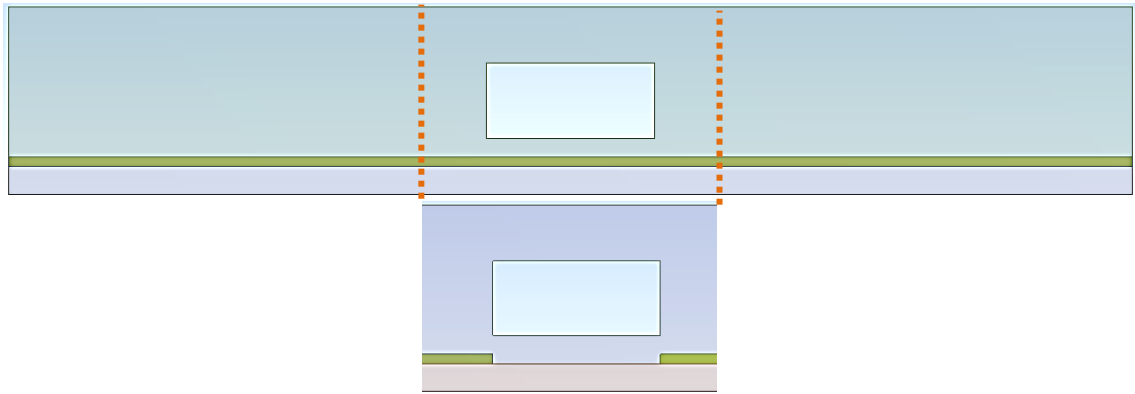


Figure 46: Geometry A (above) and detail of step for geometry B (below).

Model A	Dimensions (mm)	Volume (m ³)	Surface (m ²)
Aluminum	60x8x400	17.76 e-005	0.065688
Channel	9x4x400	1.44e-005	0.010472
Union(interface)	60x0.5x400	1.2e-006	0.04846
Copper	60x1.5x400	3.6 e-005	0.04938
Inlet and outlet	9x4	-	0.000036

Table 7: Dimensions for model A.

Model B	Dimensions (mm)	Volume (m ³)	Surface (m ²)
Aluminum	60x8x400	17.94 e-005	0.066097
Channel	9x4x400	1.44e-005	0.010472
Union(interface) (x2)	25.5x0.5x400	5.1e-006	0.020825
Copper	60x1.5x400	3.6 e-005	0.04938

Table 8: Dimensions for model B.

Concerning the mesh, preference was not an extra fine mesh which takes long time simulations, but enough fine to get accurate results. The choice made was same for every model: an adaptive mesh to every single body in addition to body sizing (0.0005 element size) for the copper, union and coolant domain. Level 1 refinement settled down for inner aluminum channel surfaces where the temperature gradient is more intense. The idea was

to establish a continuous mesh throughout the materials so the nodes in the interfaces coincide. Details are shown in Table 9 and Table 10:

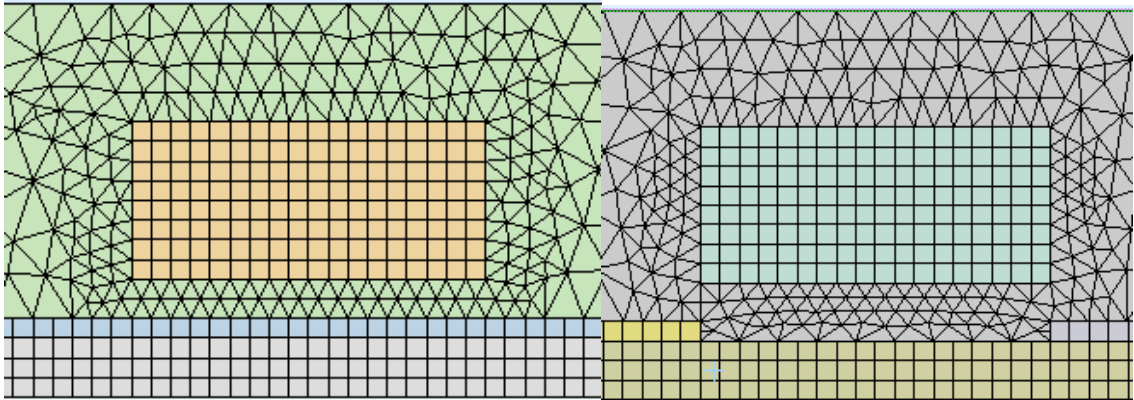


Figure 47: Mesh detail in the inlet region. Model A (left), model B (right).

Mesh Statics for Model A			
Size function	Adaptive	Span angle center	Fine
Relevance center	Fine	Bounding Box Diagonal	0.40460 m
Element size	0,001 m	Average Surface Area	6.21e-3 m ²
Initial size seed	Assembly	Minimum edge length	0,0005 m
Smoothing	High	Nodes	934876
Transition	Slow	Elements	1546693

Table 9: Mesh statics for model A.

Mesh Statics for Model B			
Size function	Adaptive	Span angle center	Fine
Relevance center	Fine	Bounding Box Diagonal	0.40460 m
Element size	0,001 m	Average Surface Area	4.41e-3 m ²
Initial size seed	Assembly	Minimum edge length	0,0005 m
Smoothing	High	Nodes	930097
Transition	Slow	Elements	1657859

Table 10 Mesh statics for model B.

5.1.2 Battery Plate Model

Battery plate geometry was proposed as a solution for battery cooling for a partner company. The batteries are in contact with the upper surface of the copper plate, proceeding to a heat conduction from the copper plate until the liquid coolant throughout the aluminum. The geometry consists in a square copper plate welded by HFSC to an aluminum structure composed of “ribs”. The ribs are mainly distributed on edges of the copper plate, with the exception of one, which is located at the center joining two surrounding ribs. The HFSC is made into four blocks of aluminum divided symmetrically among the copper lower surface. The liquid coolant moves through the inner channels, whose shape is similar to a horseshow, with a small curve and large sides. The inlet is made on the left hand side hole for each channel, so the liquid movement on the curve is always in a clockwise

direction. Both inlet and outlet are carried out perpendicularly to the plane of the copper plate, therefore is highly probable to have reverse and turbulence flow in those faces. Next table depicts the most representative parameters for the model geometry.

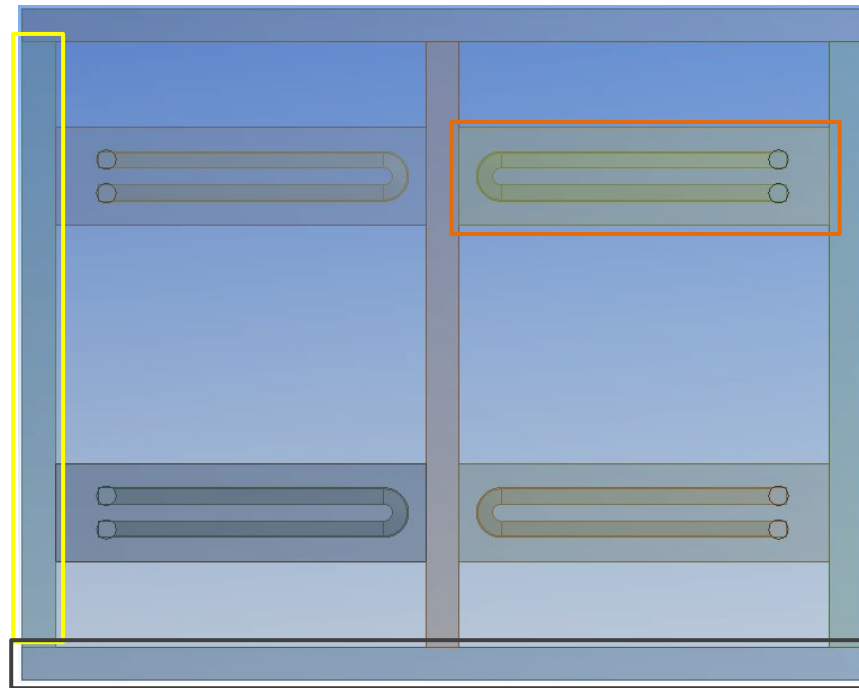


Figure 48: Top view of Battery Plate Model geometry and aluminum constituent bodies: type 1 (black), type 2 (yellow) and block (orange).

Battery Plate Model	Dimensions (mm)	Volume (m ³)	Surface (m ²)
Aluminum type 1 (x2)	20x8x500	8e-005	0.02832
Aluminum type 2 (x3)	20x8x360	5.76e-5	0.02048
Aluminum block (x4)	58x8x220	9.1047e-5	0.039566
Channel (x4)	-	1.1033e-5	0.009598
Copper plate	400x500x1	2 e-4	0.04018
Inlet and outlet	115 (diameter)	-	10.387e-5

Table 11: Dimensions for Battery Plate Model.

Difference to previous models, Battery Plate Model requires a fine and precise mesh to carry the simulation the most accurate and realistic. It was decided to use an adaptive size function with element size equal to the minimum edge length (0.0005 m). This notably increases the number of elements and nodes to analyze and so the simulation time. All aluminum ribs and copper plate generated mesh was squared while tetrahedrons shape for aluminum block and coolant domain. As seen in the figure below, mesh interfaces were coupled by matching nodes from different bodies to ease convergence and a refinement grade 1 was applied to the coolant domain interfaces. Many contact regions were automatically detected by Fluent, arranged in five groups: contact coolant-aluminum block, aluminum rib-block, aluminum rib-rib, aluminum rib-copper and aluminum block-copper. Contact regions were later coupled for a better simulation.

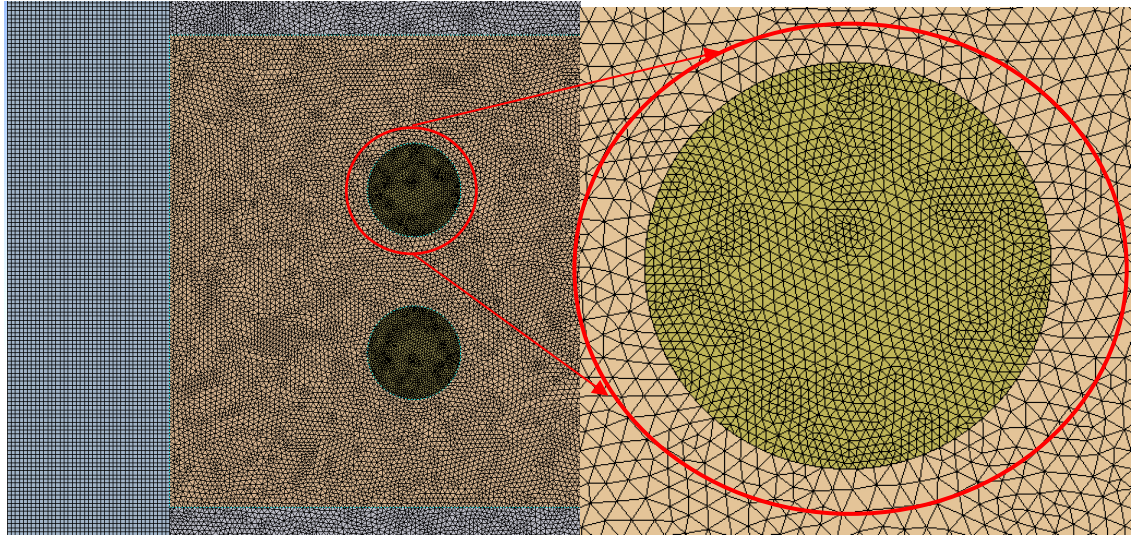


Figure 49: Mesh section and inlet detail for Battery Plate Model.

Mesh Statics for Battery Plate Model			
Size function	Adaptive	Span angle center	Fine
Relevance center	Fine	Bounding Box Diagonal	0.640380 m
Element size	0,0005 m	Average Surface Area	2.8488e-3 m ²
Initial size seed	Assembly	Minimum edge length	0,0005 m
Smoothing	High	Nodes	7386230
Transition	Slow	Elements	23398350

Table 12 Mesh statics for Battery Plate Model.

5.1.3 Network Systems Model

This geometry was proposed as a solution for power electronics cooling for a partner company. Power electronics are in contact with the upper surface of the copper plate, proceeding to a heat conduction from the copper plate until the liquid coolant throughout the aluminum. The geometry consists in a semi-rectangular copper plate fitted in an aluminum structure which also acts as a protective hood and incorporates mounting holes. Heat flux is not uniform along the copper plate as in the preliminary models. Following the specifications of the partner company, the power electronics were accurately located to meet their needs. Each component induces different heat power into the copper. The channel path was designed aiming to cover the maximum available surface around the components to cool them down. To simplify bodies and thus simulations, some parts were removed since they do not affect the thermal study. The bodies that intervene in calculations are copper (including the power electronics), aluminum and coolant.

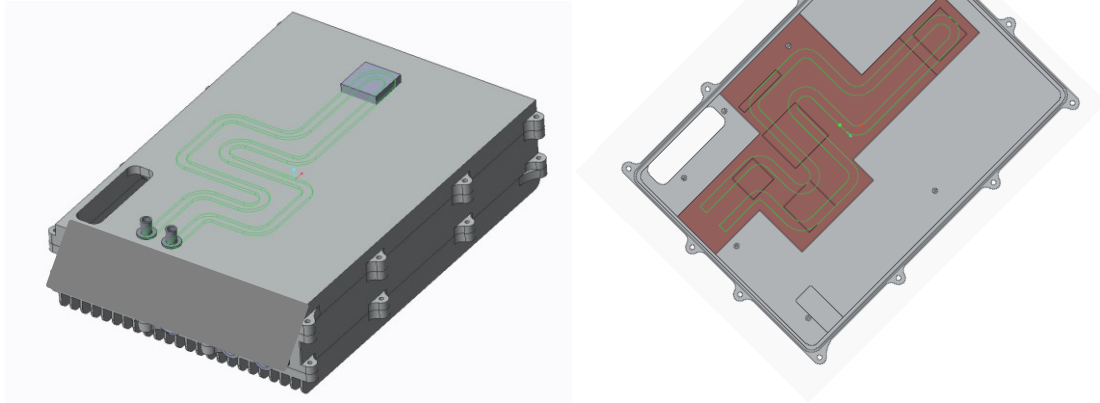


Figure 50: Prototype (left) and useful bodies (right) for the calculations.

Network Systems Model	Dimensions (mm)	Volume (m³)	Surface (m²)
Aluminum	60x8x400	17.94 e-005	0.066097
Channel	9x4x400	1.44e-005	0.010472
Copper	60x1.5x400	3.6 e-005	0.04938

Table 13: Geometrical data for Network Systems model.

Regarding the mesh, the choice made was an adaptive size function with 0.001 m of element size. A refinement was set to the components and inlet/outlet walls predicting to be the most conflicting regions in terms of simulation. Two contact regions were detected. One, contacting aluminum and coolant by 116 faces. Second, contact between aluminum and copper, touching 7 faces. It is important to say that all the power electronics are considered in the copper body, thus there are no contact regions. Both power electronics and copper plate form a solid block of continuous material.

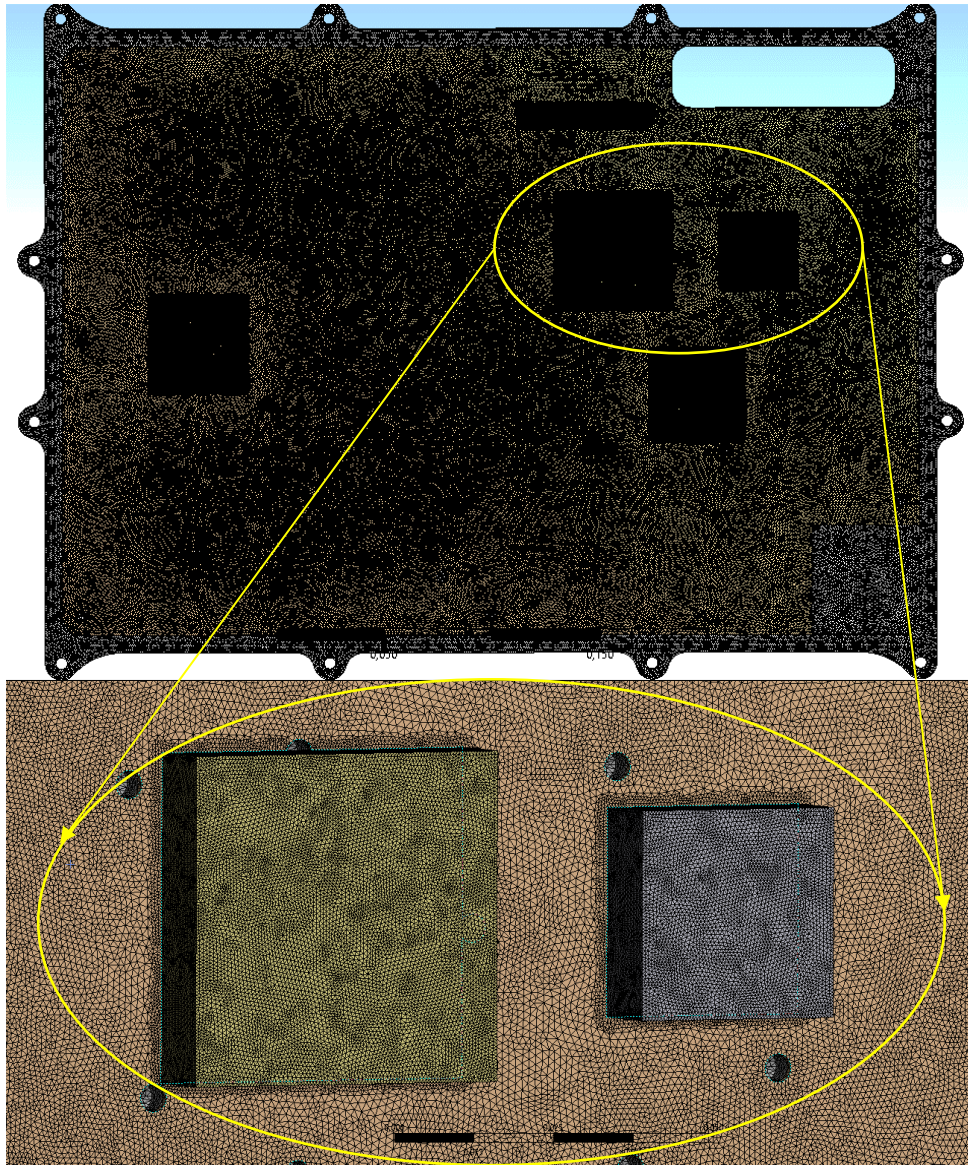


Figure 51: Mesh detail Network Systems model.

Mesh Statics for Network Systems Model			
Size function	Adaptive	Span angle center	Fine
Relevance center	Fine	Bounding Box Diagonal	0.541950 m
Element size	0,001 m	Average Surface Area	8.484e-4 m ²
Initial size seed	Assembly	Minimum edge length	5.0421e-4 m
Smoothing	High	Nodes	1578092
Transition	Slow	Elements	7432711

Table 14: Mesh statics for Network Systems model.

6 Results and discussion

This chapter shows the results of the simulations done for every model. As said before, also boundary conditions and mesh are detailed for each geometry.

6.1 *Basic model: influence of diverse parameters.*

6.1.1 Influence of roughness.

To demonstrate the advantages of HFSC, first step is understanding the influence of roughness in the channel. Roughness increases the contact surface with the liquid coolant and creates turbulent flow contributing to the heat transfer.

First model consists of a copper plate in contact with the aluminum block. In the interface, there is a new material, named as UNION, which acts the role of the thermal resistance in the interface between aluminum and copper. The properties given are shown in Table 6, being the thermal conductivity the most relevant parameter. As coolant, water was used. The goal of this first model is to evaluate the influence of roughness in heat extraction. For that purpose, model A was chosen to later analyze the benefits of the weld zone with model B. Two simulations were done: first one with no roughness on the channels and second with a 0.002 m height roughness. Despite evidence that roughness values are different depending on channel wall (roof has higher roughness than bottom, 2.3.4) it was set an average value slightly higher (to secure influence in the model) than experimentally tested by Karvinen [70] for every wall.

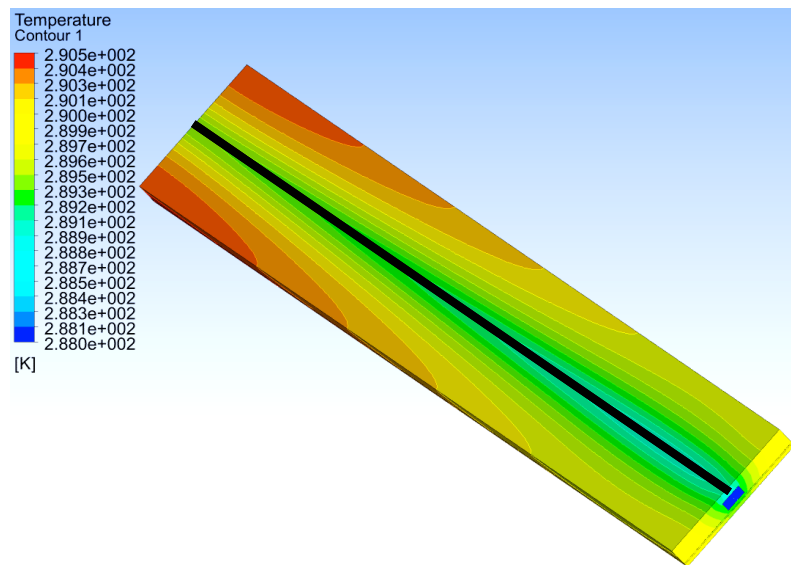


Figure 52: Temperature gradient in model A and region plotted in Table 15 highlighted in black.

To ascertain whether the temperature decreases and how much it does, the regions chosen for the estimation are located above and below the channel depending on the material. A straight line was drawn along the length of the geometry in the three regions to study: copper, aluminum and liquid coolant. Throughout this line, temperature was plot in Figure 53, where easily can be seen the temperature decrease when increasing the channel roughness. As expected, the results of the simulations demonstrate the efficacy of roughness. Despite the extra temperature removal is less than 2 degrees, which could seem such

a bad extra removal, is important to notice that the length of the channel is just 0.4 meters, a small length compared with what these channels can be. Channel length can be much higher, such in Showmik [71] study for a real battery cooling, where the length of some channels are far than 2 meters.

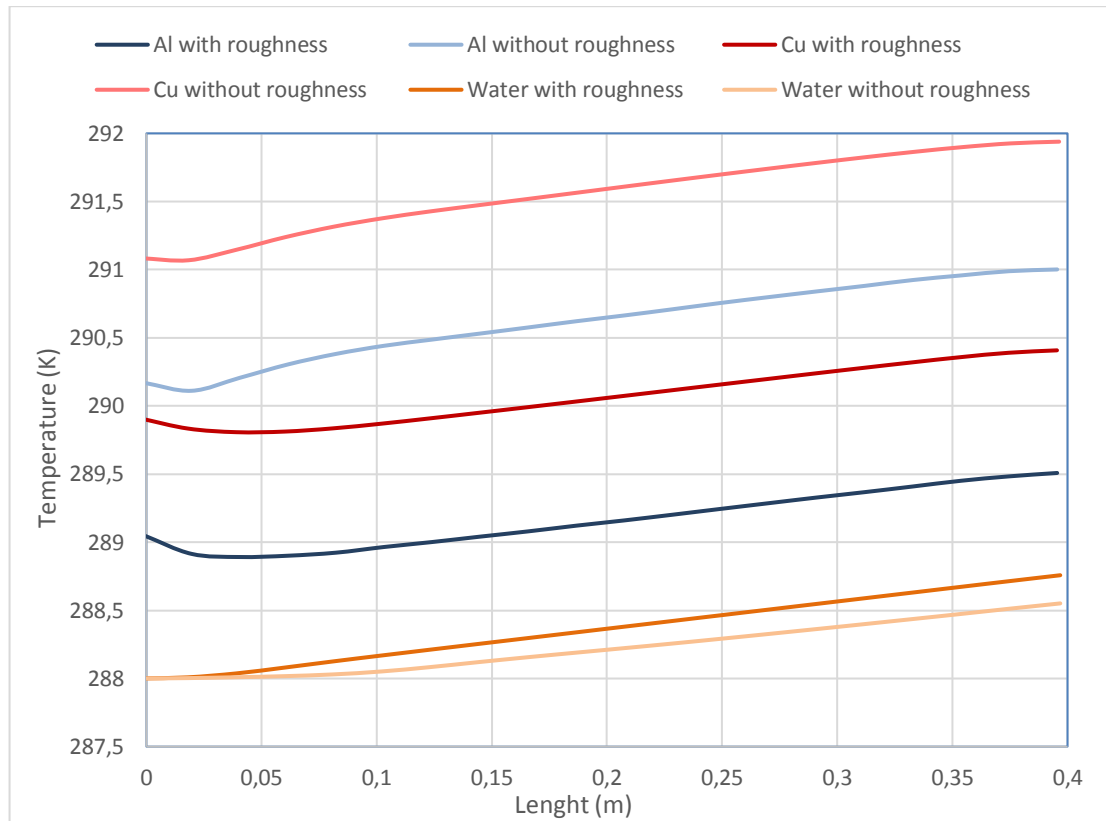


Figure 53: Temperature variation along copper and aluminum for both cases: roughness and non-roughness channel.

<i>Material</i>	Maximum temperature without roughness (K)	Maximum temperature with roughness (K)	ΔT (K)	η ($\frac{K}{m}$)
<i>Aluminum</i>	291.00	289.51	1.5	3.75
<i>Copper</i>	291.94	290.41	1.53	3.825
<i>Water</i>	288.55	288.76	-0.21	-0.525

Table 15: Difference in maximum temperature for each material.

Also, in Figure 54 is noticeable the higher turbulence created in the liquid domain. Dissipation increases quickly within the first few millimeters to then establish for the rest of the path. In turbulent flow, fluctuations produced provide an extra improvement for heat transfer thanks to the eddies formed which transport mass and energy across several regions of the flow. Laminar flows, due to the orderly particle movement along path lines, only allow heat transfer between streams through molecular diffusion. Hence, heat transfer coefficient is greater in turbulent flows. Turbulence appears when high velocities, but roughness let have turbulent flow even with low velocities.

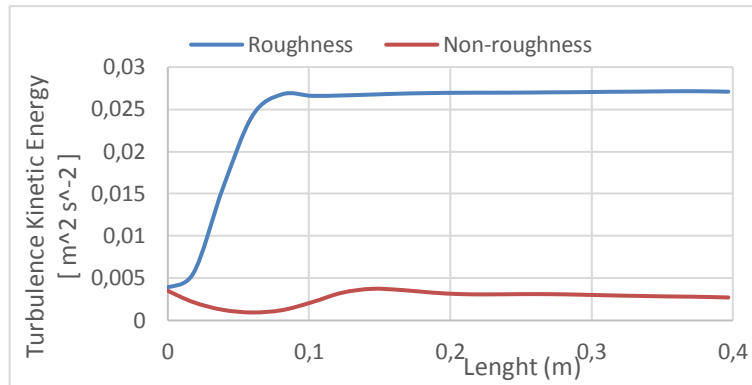


Figure 54: Turbulence kinetic energy dissipation for roughness and non-roughness channel.

To ascertain how far roughness benefits the heat transfer, a simulation with an oversized roughness of 0.03 m height was ran. It is a high value, but useful to see the changes promoted by excessive roughness. Results demonstrated a higher temperature in copper (291.8 K), which does not fit with expectations. Taking a look at kinetic energy, values are three times greater ($0.0622 \text{ m}^2/\text{s}^2$ at the maximum point). Despite having much surface area and turbulence in the flow, the answer to reach higher temperature in the copper resides on velocity. An excessive roughness could slow down the flow so the coolant gets warmer faster thus remote areas from inlet suffer from cooling effectiveness.

6.1.2 Influence of weld zone

Roughness channel is not the only advantages in HFSC. The interface when two materials in contact supposes an impediment for heat transfer. However, HFSC breaks the interface barrier by welding in solid state both materials in the region below the channel, creating a bridge for heat transfer. This chapter demonstrates the benefits of the weld zone compared with a simple contact interface.

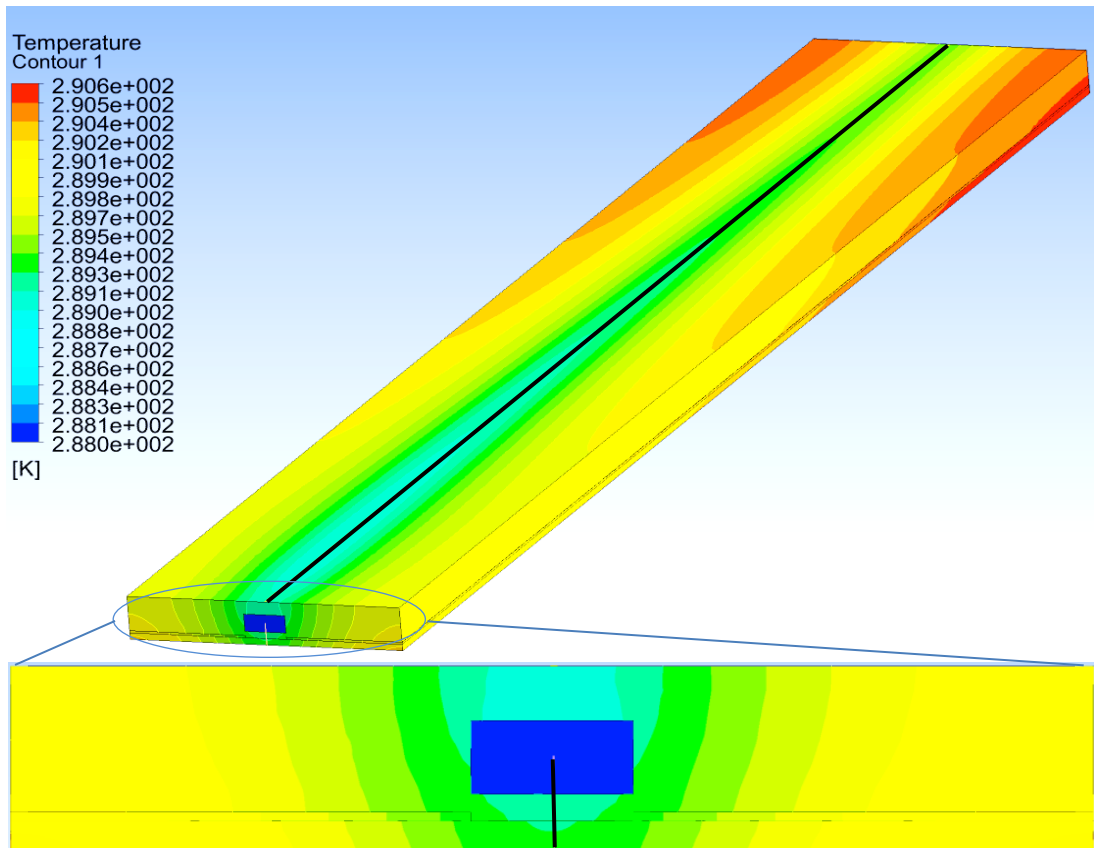


Figure 55: Temperature gradient in model B and detail of temperatures plotted (black lines)

For that purpose, model B was chosen, where the existent step combines the aluminum and copper. Same boundary conditions were set, but coupling the contact aluminum-copper. The analysis focusses on the temperature gradient along the channel and in the direction from the copper to the channel, where there is the weld zone. The results accomplished with predictions, but in a lower level than expected. In

Figure 56 we can see that the range of temperatures in the aluminum is the same for model B (weld) than for model A (interface material). Instead, is noticeable a slightly higher heat removal in copper. Heat flux is applied to the copper and the facts of having the weld joint aids for a lower temperature. Nonetheless, this difference is pretty small (0.7 K) and could no longer be considered significant.

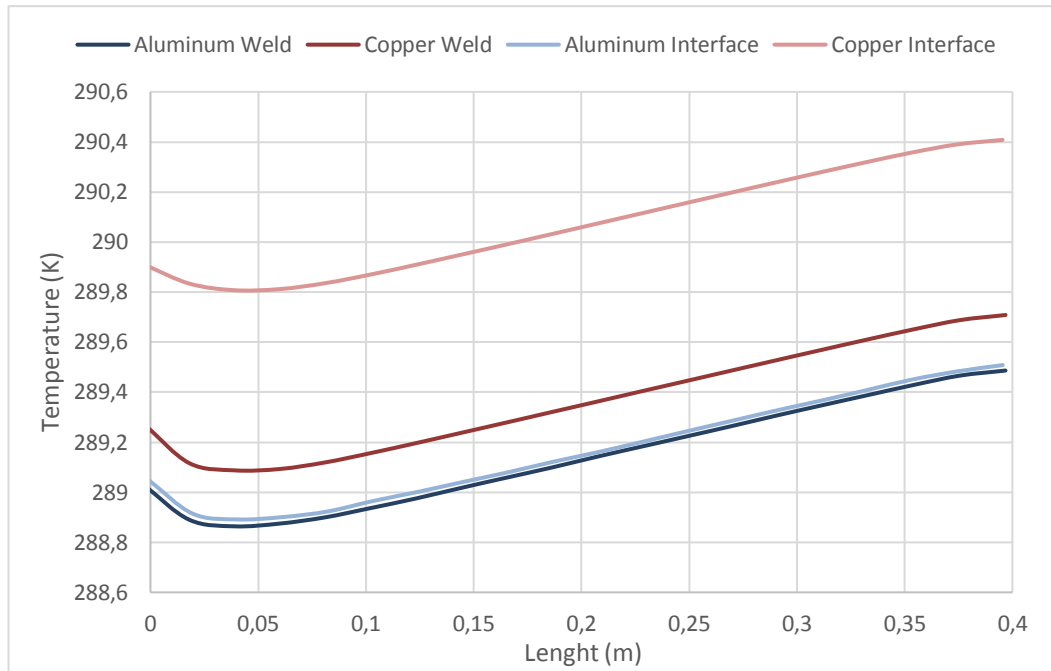


Figure 56: Maximum temperatures across body length for model B.

Most relevant information is shown in

Figure 57. It is outlined the temperature drop that takes place in the weld zone. The region to be studied corresponds to the first half of the plot, distance from the bottom of the copper to the aluminum through the weld zone. Second half of the plot shows the drop when contact with water, less important in our case of study. No matter inlet or outlet, both regions incorporate the same improvement of HFSC. The smooth transition of material properties through the weld zone compared with the interface is reflected in the temperature gradient. The drop throughout the interface is higher and thus the heat transfer to the aluminum, decreasing the efficiency of heat removal. The ease of crossing the weld zone allows a lower maximum temperature in copper surface and practically there is no thermal leap within surfaces. It is clear that an improvement of the technique could consist in widen the weld zone as much as possible to have a greater continuous region which guarantees higher heat transfer.

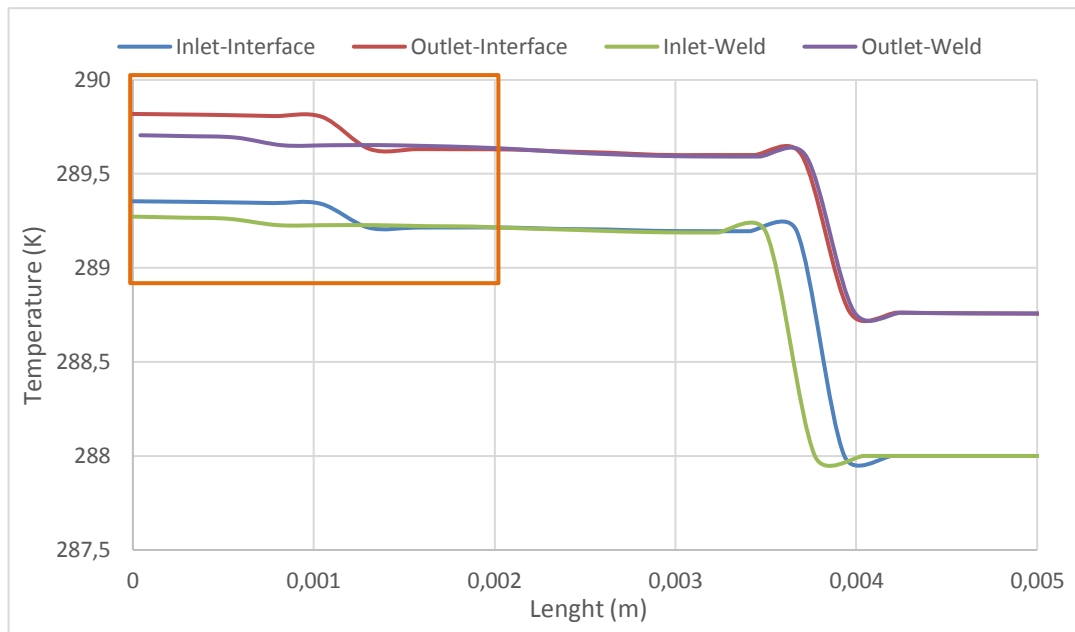


Figure 57: Temperature drop at inlet and outlet for weld and interface models.

Due to the heat input of the simulations, not enough to see great advantages of the weld zone, another simulation was run to clarify its benefits. Using the same model, the interface material named as UNION was given properties of air, typical fluid located in interface, whose thermal conductivity (0.02735 W/mK) is much lower than in the contact aluminum-copper (33.3 W/mK). This experimental set up makes easy to see the thermal bridge given by HFSC. Obviously, the thermal resistance offered by the air raises maximum temperature in the copper (295.7 K) and lows temperature in aluminum since there is less heat transfer across the UNION. Practically, the whole weld zone has same temperature thanks to the continuity in material and similarity in properties. Heat flows more quickly in that region and presents no temperature drop.

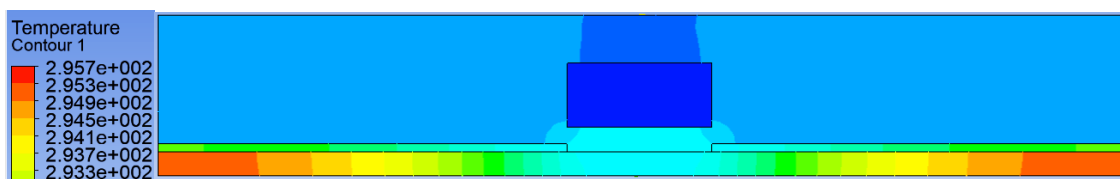


Figure 58: Heat transfer throughout the weld zone.

6.1.3 Influence of coolant velocity

Coolant velocity has an important influence in heat extraction, but also considerable limitations. Velocity is not uniform along the channel. Friction losses and path elements, such as elbows, decrease velocity directly affecting heat transfer. In a cross section, flow particles reach their faster velocity in the center of the channel, while the velocity is nearly zero in the points immediately after the walls. This phenomenon is due to viscosity, so is a parameter which will play an important role when choosing coolant properties.

It is clear that the higher the flow velocity, the higher the heat extraction. As much coolant goes along the channel, its temperature will be lower in distant locations from the inlet

and so more heat can be extracted. The velocity of particles close to the walls also increases playing a facilitating role in heat transfer. Low velocities raise the temperature flow quickly matching temperature with their surroundings losing quickly its capacity to remove heat.

To demonstrate, model B was run with different volume flows. The criteria to choose these flows is based in an experiment carried out by Karvinen [70], where the maximum and minimum volumetric flows were 0.5 l/min and 6.0 l/m. Taking these values as a reference and converting volumetric flow to velocity by means of inlet surface (Table 8) a range of velocities was selected: 0.4, 1, 1.5 and 3.5 m/s.

Figure 59 shows the results obtained for each velocity in the copper plate since it is the body where the temperature reaches maximum value. Results indicate nothing out of the ordinary: for the lowest velocity maximum temperature was the higher while the lower temperature was achieved by the highest flow. Nevertheless, should be underlined the ineffectiveness of high velocities. There is an important drop in temperature between 0.4 and 1 m/s, but once this value is exceeded, temperature drop is too small to be profitable. As velocity increases, the slope of the lines nearly disappears which means an inefficient use of the coolant. Increasing velocity 3.5 times only decreases about 1 K the copper temperature. At this point, is important to make a balance between advantages and disadvantages of high speeds. Restrictions lie in costs, space and losses. Lofty velocities require greater pumps to accomplish with the flow conditions, thus more space is needed in the geometry surroundings or whether the pump is installed and costs increase. Moreover, losses and pressures generated with these rates must be considered since can excessively alter the flow or even damage the channel.

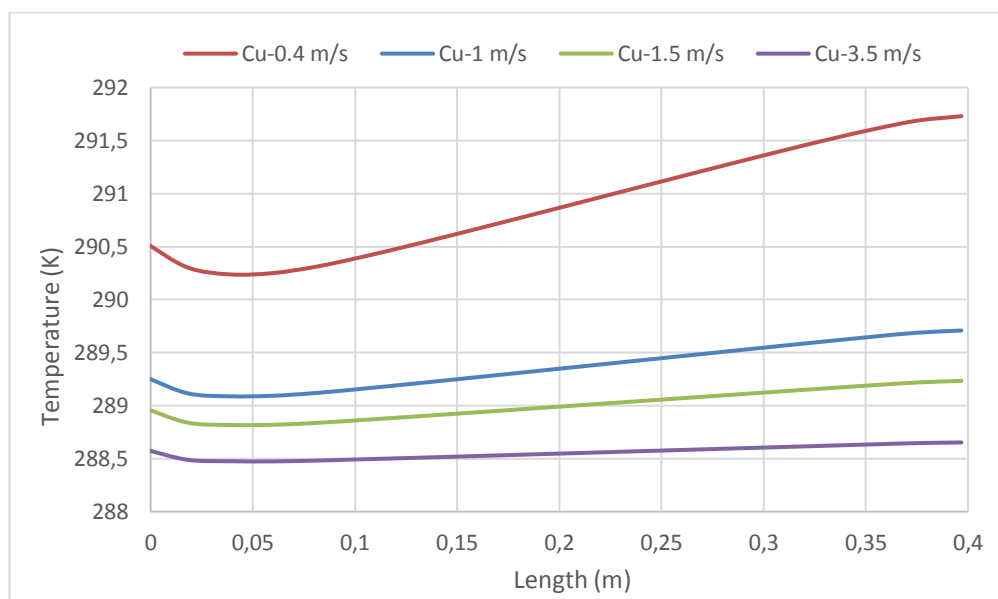


Figure 59: Temperature variation in copper for different inlet velocities.

Another issue to care about is the geometry for inlet and outlet. Our model presents a straight channel with inlet and outlet in the same plan and direction. Nonetheless, most of the designs manufactured on our laboratory required an inlet perpendicular to the upper surface of aluminum. That requirement forces the flow to make a turn favoring the appearance of reversed flow and losses which increase directly proportional to flow velocity. Optimal velocity inlet will be different for each model depending on the geometry, channel path and requirements given.

6.2 Battery plate model

When running simulation, the first problem arose in outlet faces. Flow outlet completely perpendicular to the channel produces reverse flow in outlet faces, where the velocity reaches it's highest and lowest depending which face we look at. This means some fluid particles going in opposite direction, generating eddy currents and thus great turbulence. A sum of this both factors heat the coolant reaching it maximum within outlet surface. For this reason, was preferred to set a low velocity inlet to avoid, as far as possible, this phenomenon whilst ensuring maximum surface temperature allowed.



Figure 60: Detail of inlet/outlet path and weld zone aluminum-copper in bottom.

So, 0.5 m/s was chosen for velocity inlet. Maximum temperature allowed for the components was 50 Celsius. Heat flux was set as 4500 W/m² into the top surface of copper plate. Results of the simulation show how effective HFSC is for heat exchangers applications. Figure 61 plots temperatures across the copper plate. It is clearly seen in the regions where the coolant flows. Temperature in those regions is nearly inlet temperature, 288 K, reaching the coolest possible level. In contrast, remote areas from the channel work close to the limit. Despite it is an assumable value, looking at the temperature distribution, with the highest peaks localized in determined regions could be reasonable to seek for an alternative design where the channels cover a greater surface decreasing temperature peaks. Nevertheless, design conditions limit alternative models and channel paths.

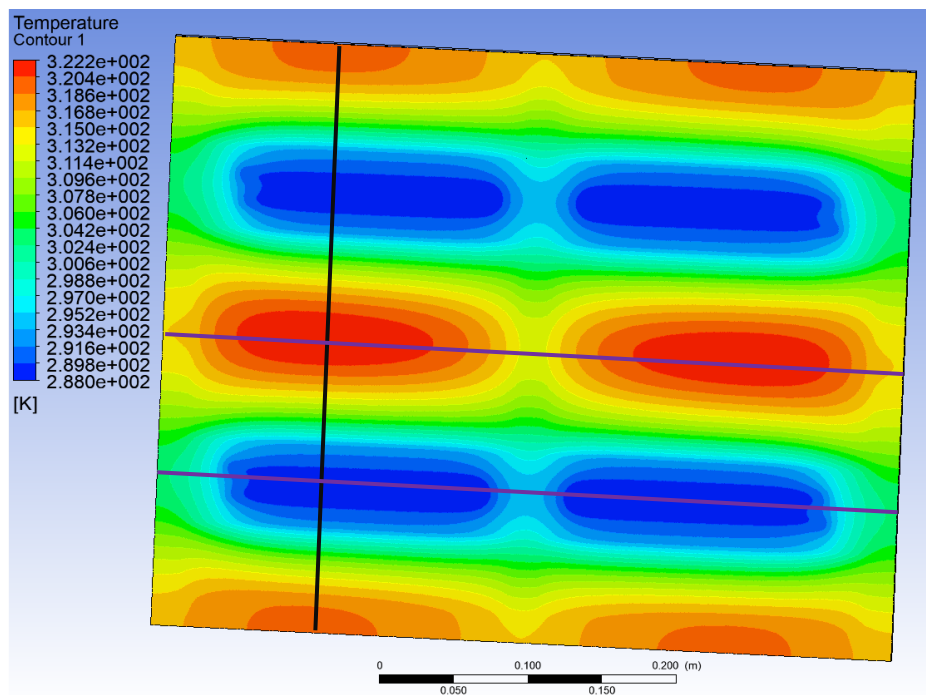


Figure 61: Temperatures in copper plate.

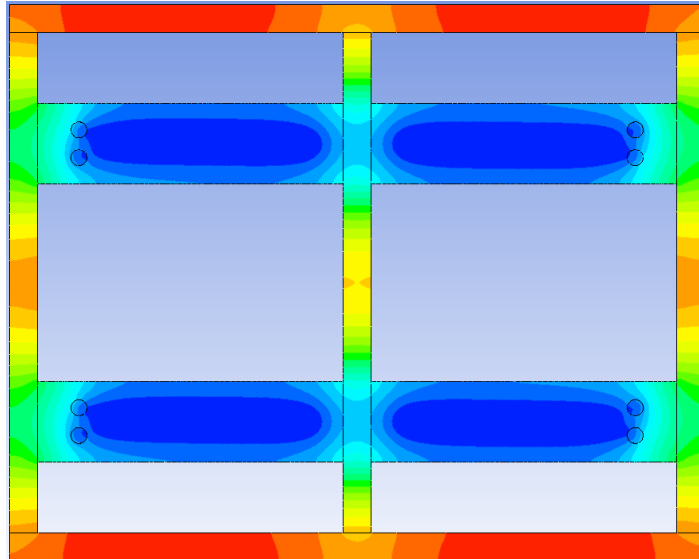


Figure 62: Aluminum parts temperature gradient in Battery Plate Model.

Next figures show the wavy variation of temperature across the width and length of the model. In Figure 61 are drawn the regions where temperatures are plot (colored lines). The below chart highlights the great difference between temperatures in regions close and remote from the channel.

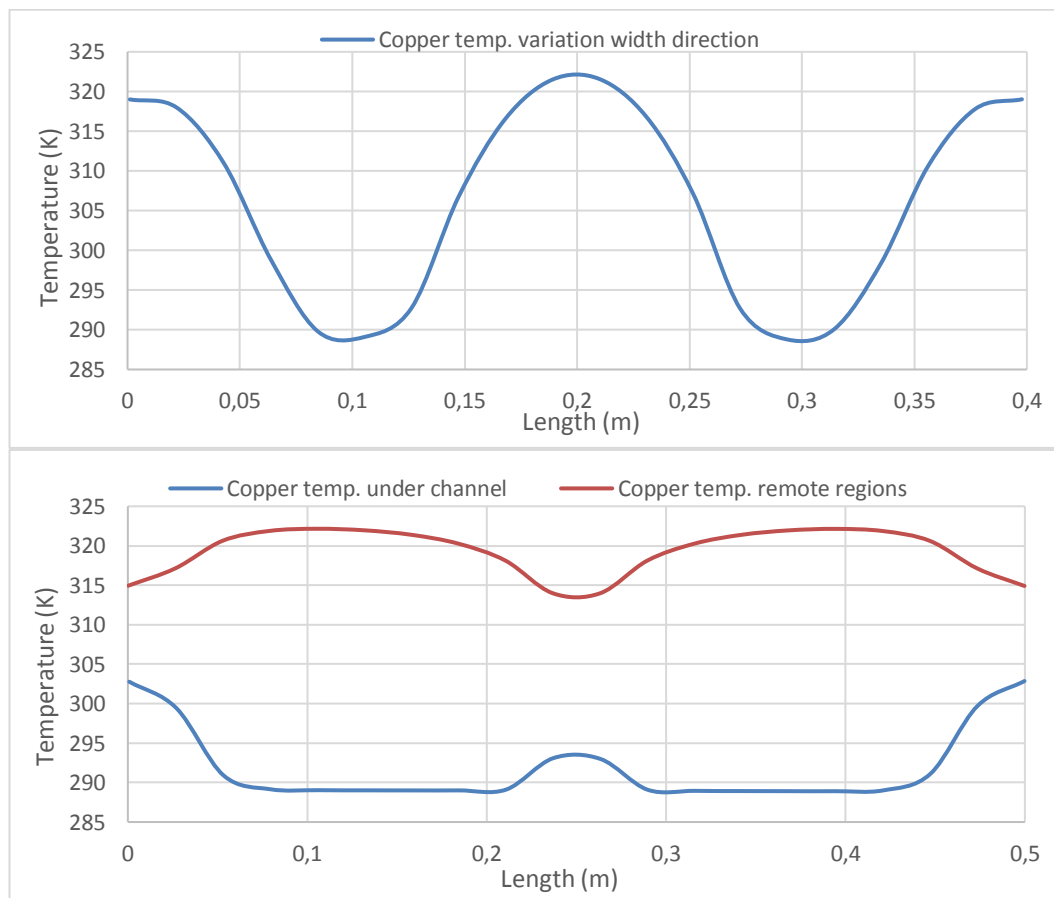


Figure 63: Plots of temperature variation throughout colored lines: above chart (black line), below chart (purple lines).

Coolant highest temperature takes places in outlet region. Coolant experiences an insignificant increase in temperature along the channel excepting the rear face in outlet. As said before, this extremely low velocity and recirculation heat the coolant and surroundings. Nonetheless, speaking in terms of efficiency, this phenomenon does not affect final results. The phenomenon occurs in a negligible volume compared to the total so scarcely will influence average coolant temperature. Furthermore, it takes place in the latest points of the coolant travel, so does not compromises the heat removal in any of the bodies as it happened in middle region. Alternatives to solve this issue are based on geometrical modifications. A smooth outlet path, with an elbow angle much lower than 90 degrees avoids particles to hardly strike the wall and consequent reverse flow. Limits in space and costs overrun reject any chance to solve this insignificant issue.

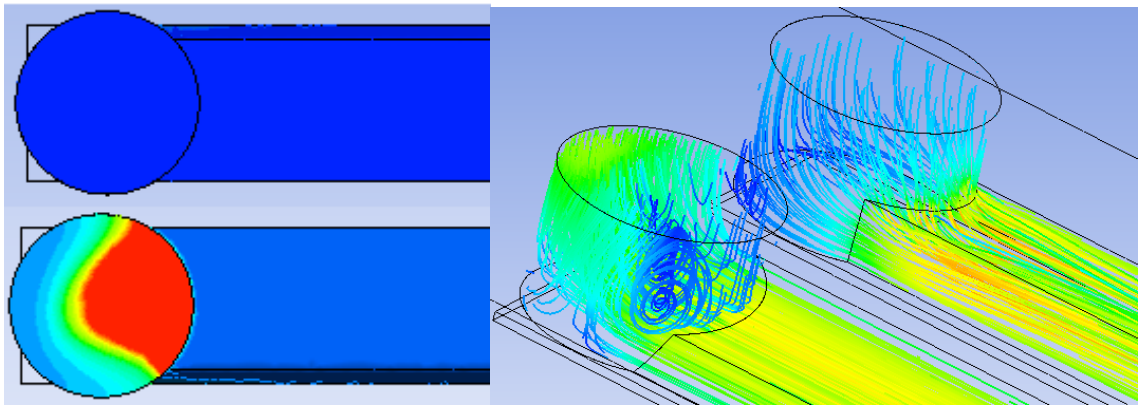


Figure 64: Flow temperature (left) and velocity streamlines showing reverse flow (right) at inlet and outlet.

6.3 *Network systems model*

The information given by partner company details the location and power of each power electronic. Although component type cannot be given due to confidential information, power for each one was given. To set that power into fluent, data was needed to be written in W/m^2 , so depending on component's surface a different value was assigned. Since there were no specifications about pump power, velocity inlet was set in an intermediate value to balance heat removal capacity and frictional losses due to turbulence flow (high Reynolds value). The heat exchanger is supposed to work in extremely different temperature conditions, varying the range from -40 to 50 Celsius. Low temperatures help to cool the plate, but for high temperatures system must be effective. The range for a proper operation of the power electronics goes to a maximum C. Thus, for the settled ambient temperature of 15C, maximum temperature to be reached is 45 C. Inlet velocity was studied for two cases (0.5 and 1 m/s) at a temperature of 288 K.

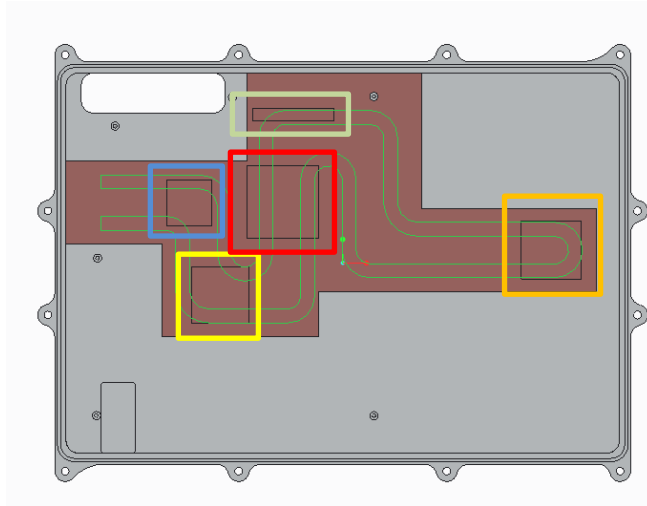


Figure 65: Power electronics location.

<i>Component</i>	<i>Surface (m²)</i>	<i>Power (W)</i>	<i>Heat flux (W/m²) (rounded value)</i>
<i>Power electronic 1 (yellow)</i>	0.001681	30	18000
<i>Power electronic 2 (blue)</i>	0.001089	30	28000
<i>Power electronic 3 (red)</i>	0.002704	50	18500
<i>Power electronic 4 (green)</i>	0.0005292	20	38000
<i>Power electronic 5 (orange)</i>	0.001849	40	22000

Table 16: Power values for each component.

At first, two simulations were done at different inlet velocities: 0.5 and 1 m/s. Both results were surprisingly optimistic since any of the velocities were able to cool down the components to a maximum temperature much lower than permitted. Figure 66 shows the values obtained. It can be seen that heat distribution is pretty similar but, as demonstrated before, the lower temperature is reached for the higher inlet velocity (1 m/s). Despite its better performing, highest velocity is not compelling since temperature decrease is less than 1 Kelvin, so it can no longer be considered the optimal operation point. Anyway, both velocities accomplish with temperature requirements.

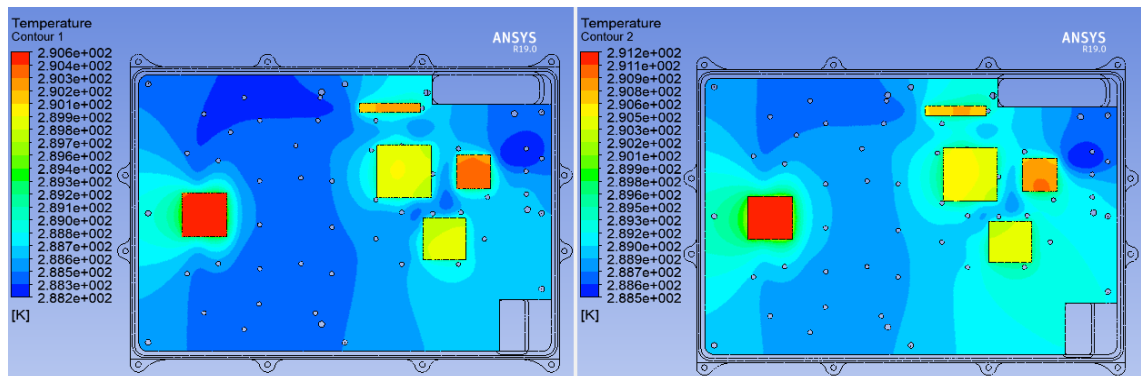


Figure 66: Temperatures in copper components for 1 m/s (left) and 0.5 m/s (right).

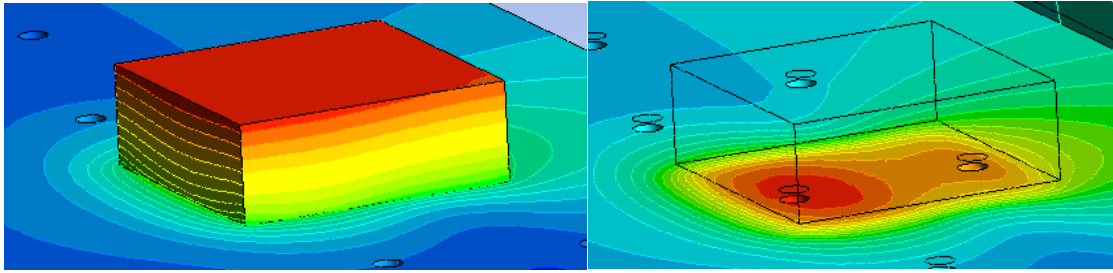


Figure 67: Temperature gradient through power electronic and contact with copper plate.

In cases where temperature difference is not relevant, other parameters must be studied to better understand why high velocities are not always the most appropriate. One of them is pressure. Figure 68 shows the pressure values in the coolant domain. In this case, the difference in pressure was substantial. Most affected region corresponds to the inlet, in which the pressure is five times higher for 1 m/s inlet velocity. Furthermore, values up to 10^4 Pa are constant throughout the coolant travel, while pressure quickly decreases to 10^3 Pa values for 0.5 m/s inlet velocity. This makes a difference: the slightly earn in heat removal does not offset the increase in pressure and frictional losses. Despite HFS channels are able to work under high pressure conditions, it is recommendable to establish low values in order to avoid flow losses in conflicting points such as joins between components of the closed fluid circuit.

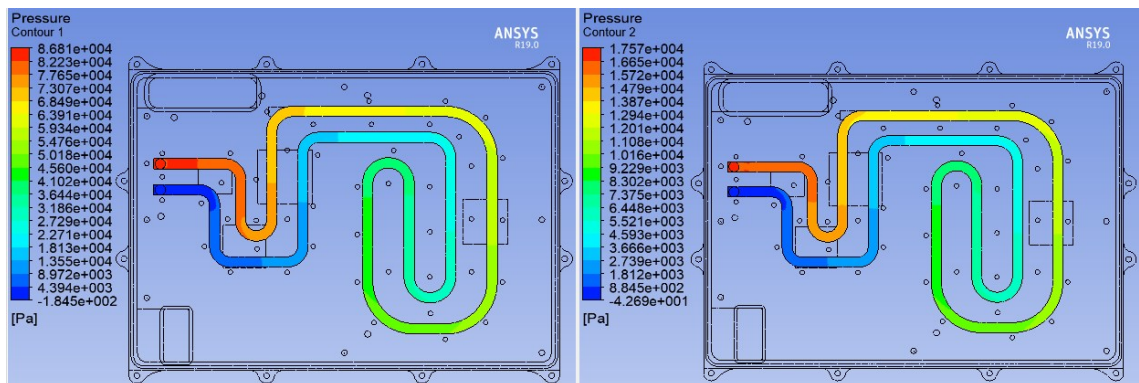


Figure 68: Pressure variation along coolant domain.

A little detail which can be considered to make optimization even finer resides in the velocity variation along channel paths. In straight sections, the coolant behavior coincides with expected: the fluid flows faster in the middle of the section while slower when close to the channel walls. Viscosity slows down flow velocity next to the walls matching the velocity of contact particles. If we have a look into any of the curves, this phenomenon behaves differently. Flow accelerates hitting the apex at high velocity while the velocity decreases on the opposite side. Moreover, when leaving the curve, forces lead the displacement of faster particles to the wall on the opposite side of the curve center. The movement is quite similar to the one made by a rider when driving into a circuit, always looking for the combination of shortest distance and highest possible velocity. Taking into account this issue, the channel could be manufactured in a way in which the power electronics are in contact with the faster flow regions. Thus, power electronics should meet the straight regions or the inner face of any curve for a better heat extraction.

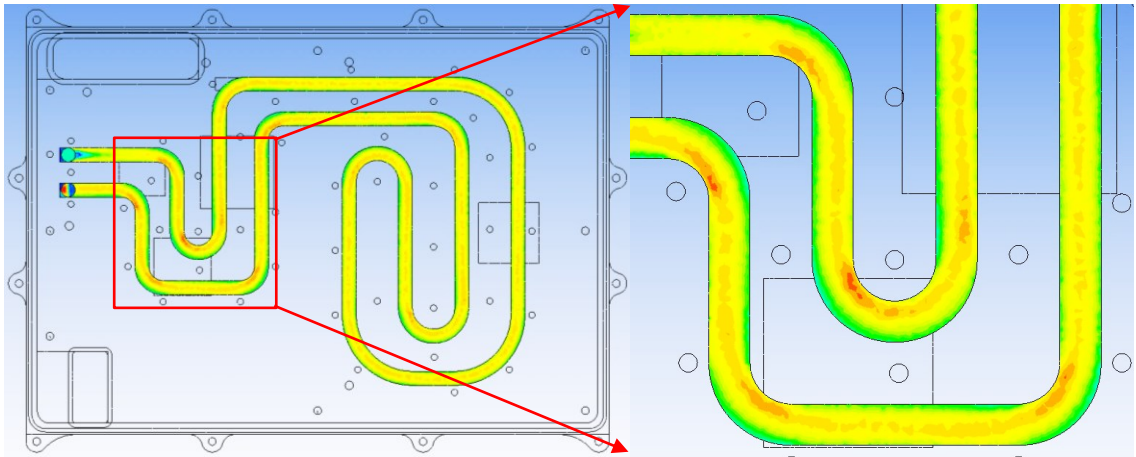


Figure 69: Velocity variation within channel curves: slow velocities (green regions) and fast velocities (orange regions).

Next figure shows velocity variation in a cross sectional section of the channel. For straight section, flow velocities are equal in their contact with the lateral walls and reach the highest velocity in the middle. On the other hand, in the curve section the peak velocity is close to the inner wall while opposite wall makes the lowest value.

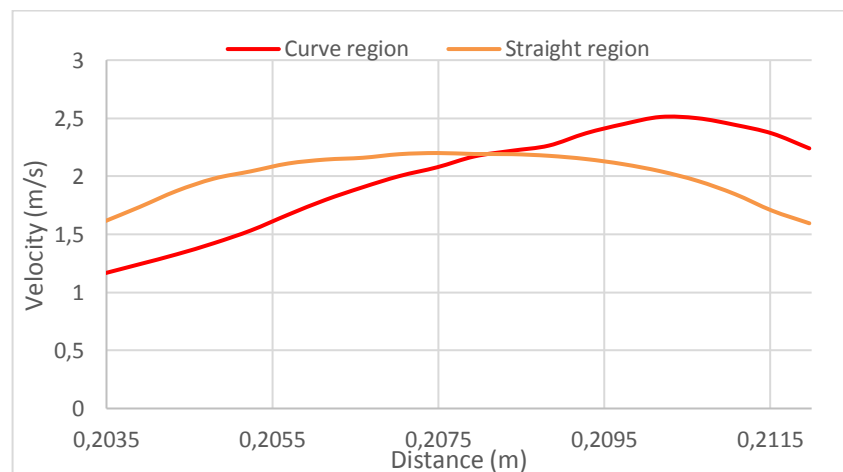


Figure 70: Velocity variation in curve and straight sections (cross section view).

In the last test made, another coolant was used instead of water. OptiCool properties are detailed in Table 5. As can be seen there, OptiCool heat capacity is lower than water, what will be determining in heat extraction. Heat capacity is the amount of heat needed to raise the system's temperature by one degree (Celsius or Kelvin). So, lower heat capacity results in easiness to get warmer. OptiCool raises temperature faster than water losing a great amount of capacity to remove heat (Figure 72). Thus, the trend is to find higher maximum temperatures in all bodies and in OptiCool. In contrast, the strength of this coolant resides in its non-electrical conductivity and viscosity. Taking into account its synthetic hydrocarbon nature, still have low viscosity to acts as heat transfer fluid. Usually, it is used in immersion cooling of electrical circuitry, but not useful in our study. Due to the higher viscosity compared with water, despite being entered to the system at same inlet velocity (0.5 m/s), the maximum temperature is lower. Viscosity difficult coolant movement and thus there are more frictional losses. By the other hand, minor velocities also mean less pressure in the channel. However, pressure decrease is not as relevant

as in previous case. Differences in temperature with water are plot in Figure 72. Next figures show maximum temperatures within the prototype.

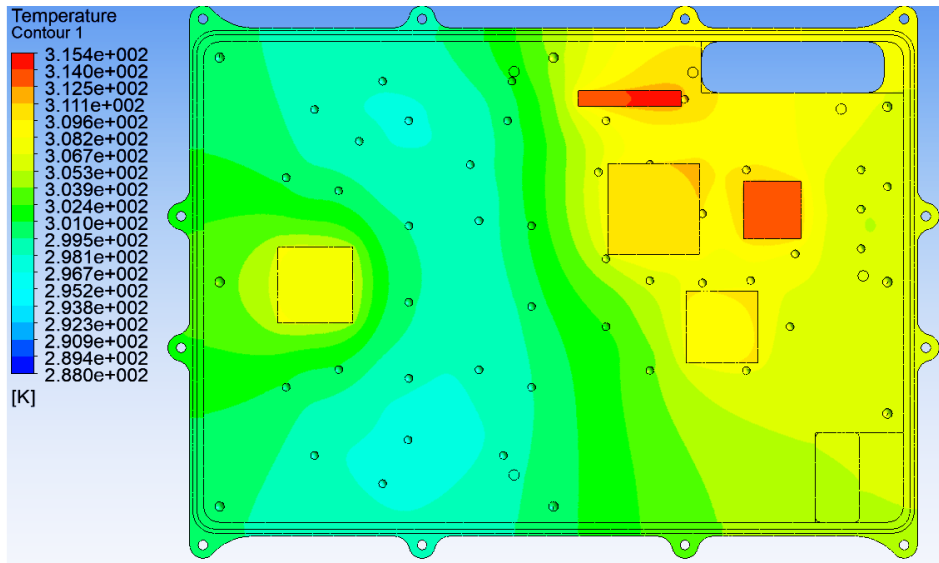


Figure 71: Network Systems prototype maximum temperatures cooled by OptiCool.

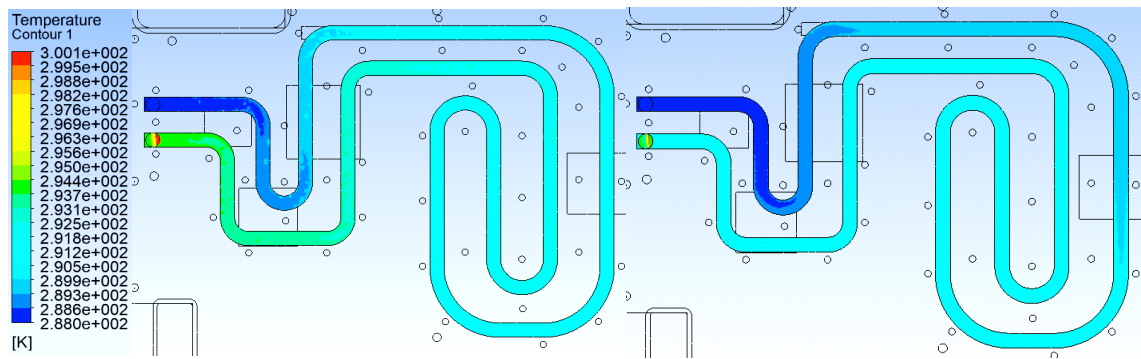


Figure 72: Coolant temperature variation: OptiCool (left) and water (right).

Finally, next table summarizes the most important values for each domain obtained during simulations.

Domain	1 m/s	0.5 m/s	0.5 m/s Opticool
Copper temperature (K)	290.56	291.22	315.4
Aluminum temperature (K)	289.77	290.43	312.41
Coolant temperature (K)	300	300	300.11
Pressure (Pa)	86805.8	17574.2	13393.1
Velocity (m/s)	2.437	1.295	1.20
Kinetic energy (m^2/s^2)	0.881	0.1959	0.1867

Table 17: Maximum temperatures in each body for different conditions.

7 Conclusions

- Friction stir welding is an environmentally friendly technique absolutely useful to weld in solid state materials with different properties by rotating a non-consumable tool which produces heat to locally soften the material by friction and plastic deformation.
- Friction stir channeling takes the opportunity to benefit from wormhole defect in FSP when inappropriate processing conditions to create continuous closed channels along different paths.
 - Channel shape, roughness and size can be modified to accomplish several requirements by varying processing tools.
 - Microstructure refinement leads to enhance mechanical and thermal properties. The finer the microstructure, the greatest the properties improvement and so capacity to work under severe conditions.
 - Hybrid friction stir channeling joins the benefits from FSW and FSC to carry a simultaneous joining and channeling in a single step operation.
- Thermal contact resistance is difficult to be determined since several factors are involved. A preliminary study on surface finish, contact pressure and material properties should be taken in each prototype for an accurate estimation of thermal contact resistance.
 - Thermal contact resistance copper-aluminum is low. The inverse value, thermal conductivity, is estimated (in standard conditions) around 33.3 W/mK, which is near the double of steel thermal conductivity.
 - Lower thermal contact resistance when heat flow from copper to aluminum (9.19 Hr*Ft²*F/BTU) than aluminum-copper (11.11 Hr*Ft²*F/BTU).
 - Smooth surfaces and high contact pressures increase thermal conductivity in the contact region as well as operating temperature.
 - Interstitial fluid also influences thermal conductivity. Typical fluid found in the gaps is air, and the amount which can be trapped within the gaps is practically negligible in heat transfer mechanism.
- HFSC provides rough inner surfaces. Roughness improves heat transfer by increasing surface area and creating turbulence in the flow.
 - Compared to a smooth surface, a standard roughness height in HFSC of 0.002 m encourages heat extraction up to 3.8 K/m depending on material properties and flow velocity.
 - Heat extraction improvement is not directly proportional to roughness height. Excessive roughness hinders flow movement throughout the channel generating unacceptable friction losses to decrease coolant velocity and its removal capacity.
 - Efficiency will depend on the balance between frictional losses and heat removal linked to roughness.
- Weld zone in HFSC contributes creating a thermal bridge throughout the contact region. Heat flow is done by conduction assisting the transfer. Temperature gets uniformly distributed in this region, the thermal leap is avoided.

- Improve achieved is not remarkable but appreciable. Lower final maximum temperature close to 1 Kelvin in each body for a small channel length.
 - Results are worse than expected. Recommended taking a test with real prototypes.
- It is preferable to high inlet velocities to enhance heat extraction efficiency. The higher the velocity the greater the heat extraction.
 - Despite lower maximum temperatures, too high inlet velocities are not recommendable due to extra pressure in the channel. Most appropriate value for cases studied within 0.5 to 1 m/s.
 - Increasing inlet velocity 3.5 times decreases maximum temperatures up to 1 Kelvin. Thermal improvement remains practically constant for inlet velocities above 1.5 m/s. Final application would determine the required velocity.
- Aggressive outlets shapes, such as perpendicular to the channel, might generate reverse flows which locally heat the water.
 - Not important influence in final result. Only if possible, the outlet shape should be smooth.
- Network Systems prototype suffers pressures five times higher when doubling the value of inlet velocity. Low pressures are preferable than small temperature drop.
 - Alternatives paths looking for the highest velocities in cross section below power electronics could maximize heat removal.
- OptiCool performs worse results than water. Temperatures are about 25 K higher than the ones achieved with water. Nevertheless, its non-electrical conductivity guarantees safety when used for electronics cooling.
 - OptiCool higher viscosity than water requires extra power to the pump for same flows.

8 Future work

Some steps can be taken for further understanding of HFSC benefits and how to extract the full potential.

- Manufacture a prototype following the standards for the models simulated for the study of the weld zone influence.
 - Prototype testing: analysis of the temperature gradient throughout weld zone and surface contact region.
 - Determination of the percentage in the composition of the weld zone.
 - Thermal contact resistance: establish the values for thermal contact resistance in our HFSC prototypes depending on the pressure applied when welding and surface finish of the incoming metal blocks.

- Cooling fins prototype: a study of suitability for power electronics using air as coolant fluid.
 - Compare prototype to HFSC efficiency.

- Prototype for electric vehicle cooling.
 - CAD design of the channel inside the aluminum block.
 - Simulation of the prototype for two different refrigerants: water and Opti-Cool.
 - Weight and costs analysis to compare with alternative technologies.

9 References

- [1] W. T. P. Vilaca, "Metadata of the chapter that will be visualized in OnlineFirst," 2011.
- [2] E. D. N. J. C. N. M. G. M. P. T. W. M. Thomas. Patent PCT/GB92/02203, 1991.
- [3] Y. L. R. F. E. T. L.E Murr, "Material Resistance Innvative," in *Vol.2*, 1998, p. 150.
- [4] J. G. a. C. V. Pedro Vilaça, "Linear Friction Based Processing Technologies for Aluminum Alloys: Surfacing, Stir Welding and Stir Channeling".
- [5] C. M. W. R. S. C.C.Bampton, "Effects of friction stir welding on microstructure of 7075 aluminum," pp. 69-75, 1997.
- [6] R. S. a. M. Z. Y. Mishra, "'Friction Stir Welding and Processing,'" 2005.
- [7] P. L. L. A. J. S. H. R. a. W. P. J. Threadgill, " "Friction Stir Welding of Aluminium Alloys,'" 2009.
- [8] M. M. B. B. M. C. a. D. B. London, "Proceedings of the Third Int. Symposium on Friction Stir Welding," Kobe, Japan, Sept 27-28, 2001.
- [9] W. Thomas, "Friction Stir Butt Welding". International Patent aplication PCT/GB92/02203 Patent 9125978,8, December 1991.
- [10] A. R. E. Thomas W M, "High performance tools for friction stir welding (FSW)". International Patent Application Patent WO 99/52669..
- [11] W. Thomas, "Friction Stir Welding". UK Patent 2,306,366, 17 Oct 1996.
- [12] W. T. C.J Dawes, "Development of Improved Tool Designs for Friction Stir Welding in Alluminium," in *Proceedings of the Fifth International Conference on Friction Stir Welding*, June 14-16 1999.
- [13] J. P. K.J Colligan, "Friction Stir Welding of Alluminium Using a Tappered Shoulder Tool," in *Friction Stir Welding and Processing*, 2005.
- [14] K.Colligan, "Tapered Friction Stir Welding Tool". US Patent 6,669,075, 30 Dec 2003.
- [15] P. T. E. S. D. S. C.J Dawes, "Development of the New Friction Stir Technique for Welding Aluminium-Phase II," TWI member report 5651/35/95, Nov. 1995.
- [16] J. X. J. P. K.J Colligan, "Welding Tool and Process Parameter Effects in Friction Stir Welding of Aluminium Alloys," in *Friction Stir Welding and Processing II*, 2003, pp. p 181-190.
- [17] J. X. R. R. K. C. J. F. J. P. S.P Vaze, "Friciton Stir Processing of Aluminium Alloy 5038 Plate for Cold Bending," in *Mater. Sci. Forum*.
- [18] J. B. K. C. R.W. Fonda, "Texture and Grain Evolutions in a 2195 Friction Stir Weld," in *Proceedings of the Fifth International Conference on Friction Stir Welding*, Metz, France, 2004.
- [19] S. L. J. d. S. T. D. F. B. T. L. D. R. Zettler, "A Study of Material Flow in FSW of AA2024-T351 and AA6056-T4 Alloys," in *Proceedings of the Fifth International Conference on Friction Stir Welding*, Metz, France, 2004.
- [20] D. S. I. R. F. W.M. Thomas, "Friction Stir Welding Tools and Developments," in *FSW Seminar*, Porto, Portugal, Dec 3, 2002.
- [21] E. N. S. W.M. Thomas, "Friction Stir Welding-Tool Developments," in *Proceedings of the TMS 2001 Aluminium Automotive and Joining Sessions*, 2001.

- [22] T. N. C. S. R. S. S. P. C.D. Sterling, "Friction Stir Welding on Quenched and Tempered C-Mn Steel," in *Friction Stir Welding and Processing*, 2003, pp. 165-171.
- [23] P. O. R.J. Ding, "Autoadjustable Pin Tool for Friction Stir Welding". U.S. Patent 5893507, 13 April 1999.
- [24] R. Ding, "Force Characterization on the Welding Pin of a Friction Stir Welding Retractable Pin-Tool Using Aluminum -Lithium 2195," in *Proceedings os the Second International Conference on Friction Stir Welding*, June 26-28, 2000.
- [25] W. M. Mahoney, "Tool Development for Friction Stir Welding," Rockwell Scientific Co., 2002.
- [26] M. W. M. Rajiv S. Mishra, *Friction stir welding and processing*, ASM International, 2007.
- [27] R. S. T. N. C. S. S. P. M. Collier, "Grade Development of Polycrystalline Cubic Boron Nitride for Friction Stir Processing of Ferrous Alloys," *Proceedings of the Fourth Internation Conference on Friction Stir Welding*, May 14-16, 2003.
- [28] W. S. B. G. R. W. T.J. Lienert, "Friction Stir Welding Studies on Mild Steel," pp. 1-9, 2003.
- [29] T. N. S. P. R. S. C.D Sorenson, "Innovative Technology Application in FSW of High Sooftening Temperature Materials," Sept 14-16, 2004.
- [30] A. B. R. J. W.M Thomas, "Skew-Stir Technology," in *Proceedings of the Third International Conference on Friction Stir Welding*, Kobe, Japan, Sept 27-28, 2001.
- [31] S. D. W. T. E. L.-C. S. B. G.M.D. cantin, "Friction Skew-Stir Welding of Lap Joints in 5083-O Aluminium," in *Sci. Technolo. Weld. Join*, 2005, pp. 268-280.
- [32] D. S. K. J. P. E. W.M. Thomas, "Com-Stir-Compound Motion for Friction Stir Welding and Machining," Cambridge, UK, 2003.
- [33] W. Thomas, *Friction Stir Welding-Recent Developments*, Madrid, Spain: TMS, 2003.
- [34] D. S. W. T. E. T. C.J Coodfellow, "Preliminary Trials Using Dual-Rotation Stir Welding," in *Romanian Welding Society Conference*, Galati, Romania, 2005.
- [35] D. S. E. W. I. N. W.M. Thomas, "The Simultaneous Use of Two or More Friction Stir Welding Tools," TWI Ltd report, Cambidge, UK, Jan 13, 2005.
- [36] W. T. C.J. Dawes, in *Weld. J.*, 1996, p. 41.
- [37] W. T. C. Dawes, "Friction stir process welds aluminium alloys," p. 41–45.
- [38] C.Bird, "Ultrasonic Phased Array Inspection Technology for the Evaluation of Friction Stir Welds," in *Proceedings of the Fourth International Conference on Friction Stir Welding*, Park City, UT, 2003.
- [39] S. L. A.J. Leonard, "Flaws in Friction Stir Welds," in *Proceedings of the Fourth International Conference on Friction Stir Welding*, Park CItY, UT, 2003.
- [40] R. Mishra, "Friction stir welding and processing," in *Friction stir welding and processing*, Materials Science and Engineering Reports, 2005, pp. 1-78.
- [41] S. S. R. M. Z.Y. Ma, "Effect of multiple-pass friction stir processing on microstructure and tensile properties of a cast aluminum–silicon alloy," *Scripta Materialia*, pp. 1623-1626, 2006.
- [42] T. McNelley, "Friction stir processing: refining microstructures and improving properties," *Revista de Metalurgia*, vol. 46, pp. 149-156, 2010.

- [43] Z. Ma, "Friction stir processing technology – a review," *Metallurgical and Materials Transactions*, vol. 39, pp. 642-658, 2008.
- [44] P. A. M.K.B. Givi, "Advances in Friction Stir Welding and Processing," Woodhead Publishing, Amsterdam, 2014.
- [45] C. W. S. P. M. R. H. Su, "Simultaneous measurement of tool torque, traverse force and axial force in friction stir welding," *Journal of Manufacturing Processes*, pp. 495-500, 2013.
- [46] C. B. D.G. Hattingha, "Characterization of the influences of FSW tool geometry on welding forces and weld tensile strength using an instrumented tool," *Journal of Materials Processing Technology*, pp. 46-57, 2008.
- [47] K. S. S. P. R. Kumar, "Process forces and heat input as function of process parameters in AA5083 friction stir weld," *Transactions of Nonferrous Metals Society of China*, pp. 288-298, 2012.
- [48] e. a. K.S. Arora, "Effect of process parameters on friction stir welding of aluminum alloy 2219-T87," *The International Journal of Advanced Manufacturing Technology*, pp. 941-952, 2010.
- [49] J. A. J.T. Khairuddin, Principles and thermo-mechanical model of friction stir welding, *Welding Processes*, 2012.
- [50] T. L. Y. Huang, "Advances in ultrafine-grained materials," *Materials Today*, pp. 85-93, 2013.
- [51] H. Conrad, "Grain size dependence of the plastic deformation kinetics in Cu," *Materials Science and Engineering A*, vol. 341, pp. 216-228, 2003.
- [52] S. C. W. G. T. Z. Z.W. Chen, "Microstructure development during friction stir processing of Al-7Si-0.3Mg cast alloy," in *8th International Friction Stir Welding Symposium, Timmendorfer Strand, Germany*, 2010.
- [53] M. T. F.C. Liu, "Microstructural evolution and superplastic behavior in friction stir processed Mg–Li–Al–Zn alloy," *Journal of Materials Science*, vol. 48, pp. 8539-8546, 2013.
- [54] R. M. K. K. N. Balasubramanian, "Friction stir channeling: Characterization of the channels," *Journal of Materials Processing Technology*, vol. 209, no. 8, pp. 3696-3704, 21 April 2009.
- [55] R. Mishra, "Integral channels in metal components". US Patent 6,923,362, 2 August 2005.
- [56] T. WM, "An investigation and study into friction stir welding of ferrous-based material," University of Bolton, 2009.
- [57] C. V. P. Vilaça, "Modular adjustable tool and correspondent process for opening continuous internal channels in solid components". Patent 105628, 15 April 2011.
- [58] P. V. Catarina Vidal, "Processo de Abertura de Canais Internos Contínuos em Componentes Maciços Sem Alteração da Cota de Superfície Processada e Respectiva Ferramenta Modular Ajustável". Patent 105628, 15 April 2011.
- [59] M. F. S. Ferraz, "Friction Stir Channeling Industrial Applications: Prototype Design and Production," Universidade Técnica de Lisboa, Lisboa, May.
- [60] W. Arbogast, "Modeling friction stir joining as a metal working process," *Hot Deformation of Aluminum Alloys*, vol. III, p. 313–327, 2003.
- [61] V. I. P. V. C. Vidal, "Mechanical Characterization of Friction Stir Channels under Internal Pressure and In-Plane Bending," in *Key Engineering Materials*, 2012, pp. 105-108.

- [62] V. I. P. V. C. Vidal, "Metallographic Characterization of Friction Stir Channels," in *VI International Materials Symposium (MATERIAIS 2011)*, Guimarães, Portugal, 2011.
- [63] D. Nordal, "Design, Development and Analysis of Tools for Hybrid Friction Stir Channeling," Dissertation for the Degree of Master of Science in Mechanical Engineering, Espoo, 2017.
- [64] "Thermopedia A-to-Z Guide to Thermodynamics, Heat & Mass Transfer, and Fluids Engineering," Thermopedia, 2 February 2011. [Online]. Available: <http://www.thermopedia.com/content/1188/>. [Accessed 11 May 2018].
- [65] M. Y. M. B. H. Mantelli, "Thermal Contact Resistance".
- [66] W. E. S. Jr., "Determination of thermal contact resistance between metals using a pulse technique," Doctoral Dissertation, 1972.
- [67] A. Inc, ANSYS 16 Fluent User's Guide, 2015.
- [68] "OptiCool Heat Transfer Fluids," DSI Ventures, [Online]. Available: <http://dsiventures.com/wp-content/uploads/2013/09/OptiCool-Brochure.pdf>. [Accessed 20 5 2018].
- [69] "Thermtest," Thermtest Thermophysical Instruments, [Online]. Available: <https://thermtest.com/materials-database>.
- [70] D. N. P. V. Heikki Karvinen, "New Development and Testing of FSChanneling Technique: HybridFSC," in *10th International Conference on Trends in Welding Research*, Tokyo, Japan, 2016.
- [71] S. Dasgupta, "Modelling and testing of hybrid channeling plates for thermal management of batteries for electrical vehicles," Aalto University, Espoo, 2017.
- [72] K. J. C. W. W.M. Thomas, "Friction Stir Welding – Recent Developments in Tool and Process Technologies," vol. Volume 5, no. Issue 7, pp. 485-490, 2003.
- [73] Z. C. D. Lohwasser, Friction stir welding From basics to applications, New York: Wood head publishing limited, 2010.

